Quantum transport in Dirac semimetal based Josephson junctions

Caizhen Li

School of Physics, Beijing Institute of Technology

2023.09.29

Contents

- **Background**
- **Synthesis and characterization of Dirac semimetal Cd_3As_2 nanostructures**
- **Transport properties of Cd_3As_2 nanostructures**
- **Results in Cd_3As_2-based Josephson junctions**
- **Summary**

Majorana fermion

Ettore Majorana

1928:Dirac equation (spin-1/2 fermion)

$$i\hbar\frac{d\psi}{dt} = c\alpha\cdot p + mc^2\beta \qquad \alpha = \begin{pmatrix} & \sigma \\ \sigma & \end{pmatrix},\ \beta = \begin{pmatrix} I & \\ & -I \end{pmatrix}$$

$\psi^\dagger \neq \psi \Longrightarrow$ charged, particle ≠ anitiparticle

1937: When α is real, β is complex, then $\psi^\dagger = \psi$

→ Majorana fermion, **zero charge, particle = anitiparticle**

In condensed matter physics, Majorana quasiparticle excitations can appear like Majorana zero energy bound state or Majorana zero mode.

Superconductor:

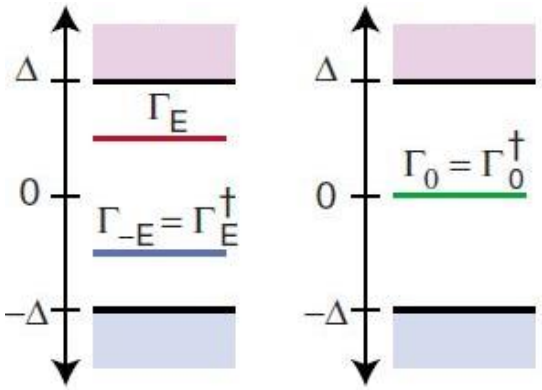

Conditions of superconductor for Majorana：

- S-wave pairing：

$$d = ac_\uparrow^\dagger + bc_\downarrow$$
$$d^\dagger = a^\dagger c_\uparrow + b^\dagger c_\uparrow^\dagger$$

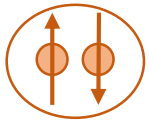

⇨ $d \neq d^\dagger$

- P-wave pairing：

$$d = ac_\sigma^\dagger + a^\dagger c_\sigma$$
$$d^\dagger = a^\dagger c_\sigma + ac_\sigma^\dagger$$

⇨ $d = d^\dagger$

Majorana zero mode

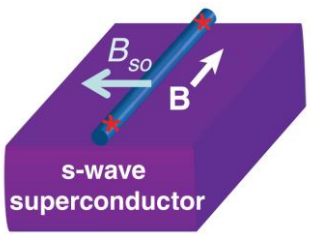

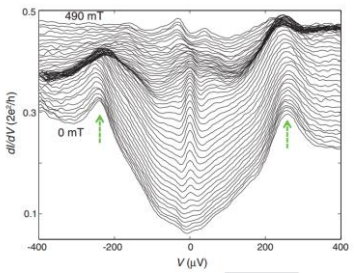

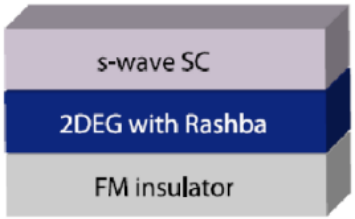

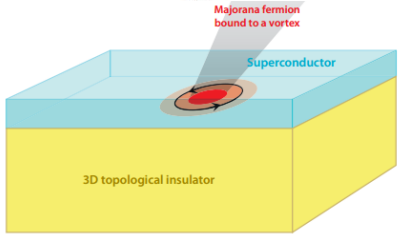

MZM in the vortex core

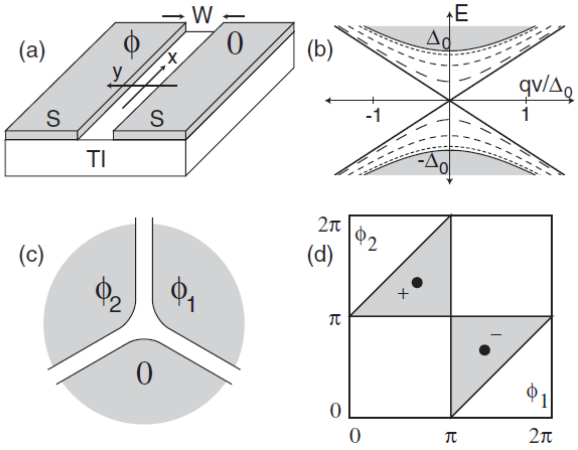

Fu-Kane proposal

Possible systems for Majorana zero modes：

- p-wave superconductor
- Fractional quantum Hall system （5/2）

Artificial p-wave superconductivity：

- Semiconductor nanowire / superconductor
- 2D electron gas / superconductor
- **Topological insulator / superconductor (2008,Fu and Kane)**
- **Topological semimetal / superconductor**

Topological insulator

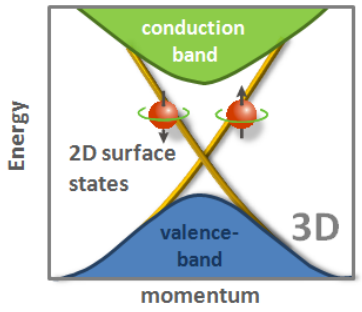

Topological semimetal

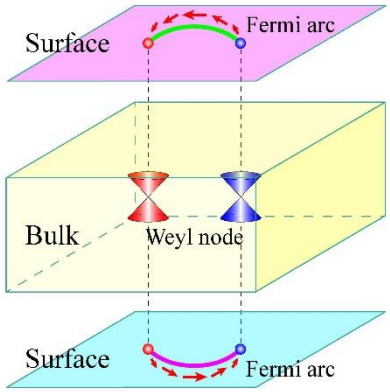

Ref：

V. Mourik *et al.*, *Science* **336**, 1003-1007 (2012).

C. Liu *et al.*, National Science Review 1, 36-37 (2014) .

C.W.J. Beenakker, *Annual Review of Condensed Matter Physics* **4**, 113-136 (2013).

Phys Rev Lett 100, 096407 (2008).

Topology

What is topology:

Topology, branch of mathematics. Topology studies properties of spaces that are invariant under any continuous deformation. It is sometimes called "rubber-sheet geometry" because the objects can be stretched and contracted like rubber, but cannot be broken.

Two objects are considered equivalent if they can be continuously deformed into one another through such motions in space as bending, twisting, stretching, and shrinking while disallowing tearing apart or gluing together parts.

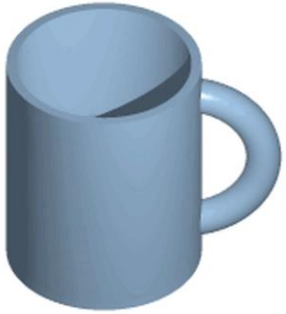

A continuous transformation can turn a coffee mug into a donut. Hence a coffee mug is topologically equivalent to a donut.

Topology

What is topology:

Topology, branch of mathematics. Topology studies properties of spaces that are invariant under any continuous deformation. It is sometimes called "rubber-sheet geometry" because the objects can be stretched and contracted like rubber, but cannot be broken.

Two objects are considered equivalent if they can be continuously deformed into one another through such motions in space as bending, twisting, stretching, and shrinking while disallowing tearing apart or gluing together parts.

genus:

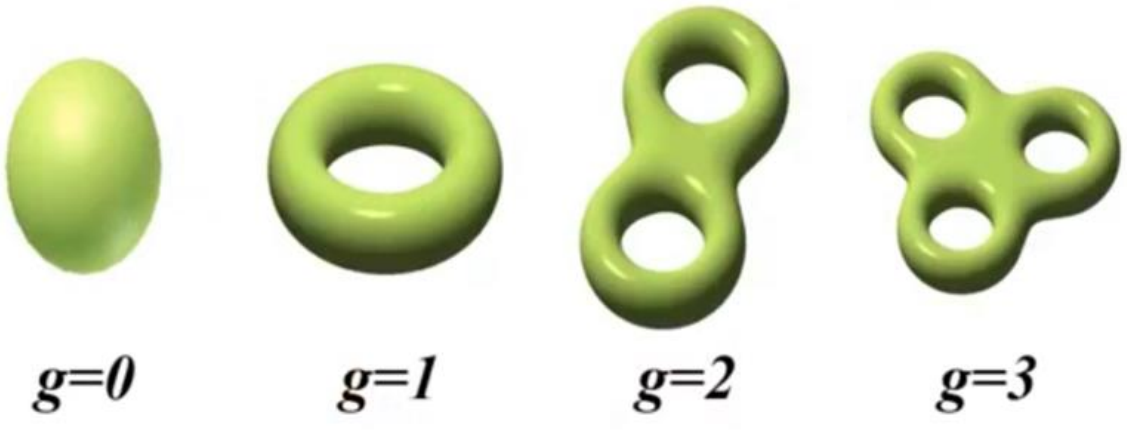

Classification of materials

metal

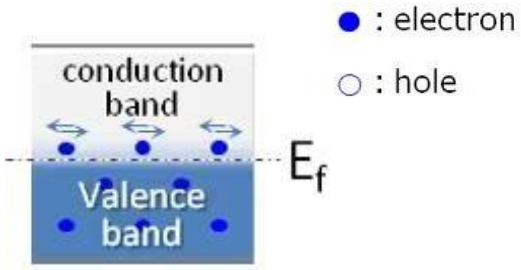

metal

semiconductor

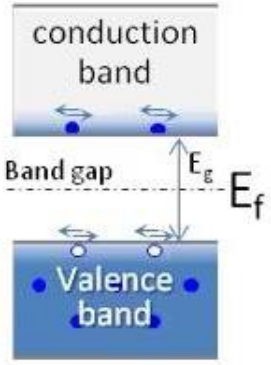

semiconductor

insulator

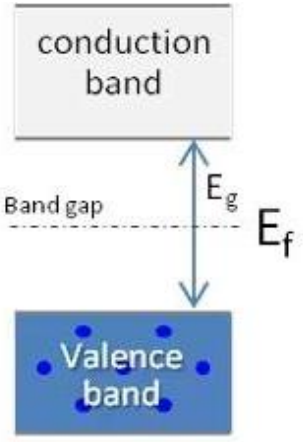

insulator

Topological Insulator

➢ **Topological insulator:**

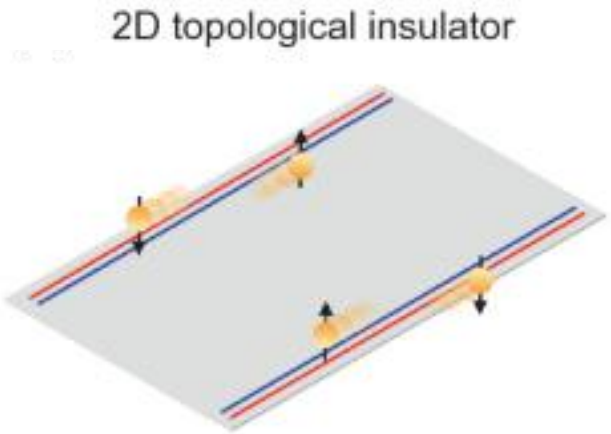

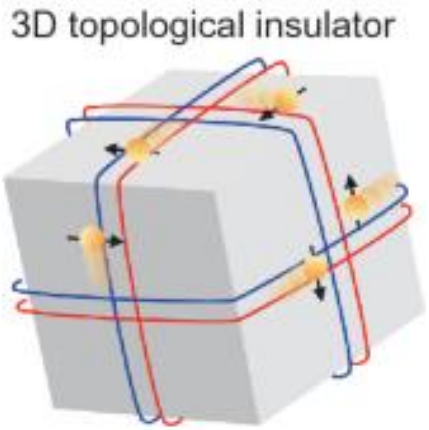

Properties:

- Bulk behaves as an insulator, while the surface behaves as a conductor.
- The surface states are topologically protected, and prevented from back-scattering
- Spin-momentum locking
- High mobility, low power dissipation

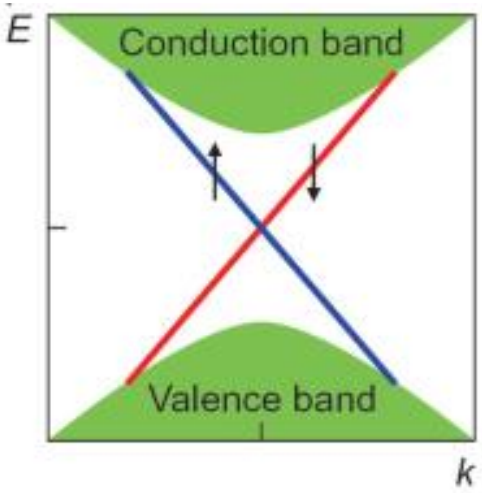

Dirac band

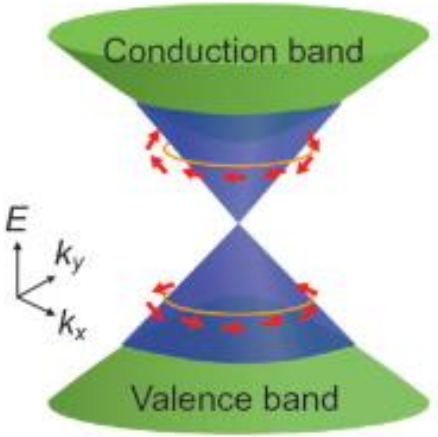

Dirac cone

Topological Dirac semimetal

➢ Topological Dirac semimetal

3D bulk Dirac band

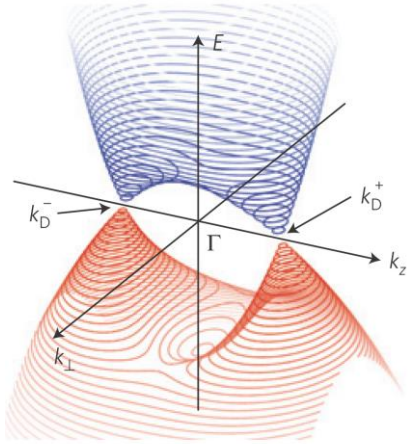

Fermi-arc surface states

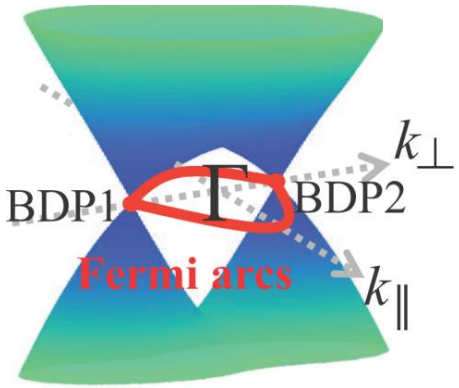

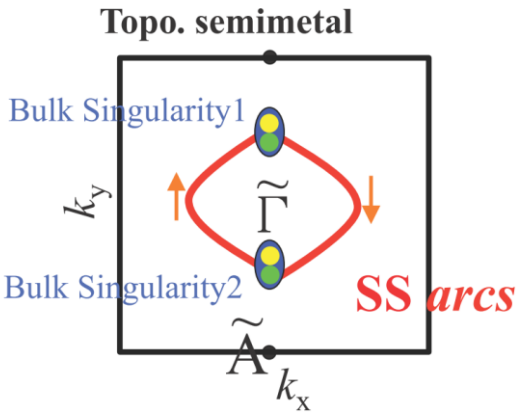

Also be called
“3D graphene”

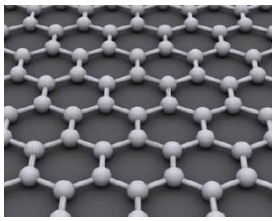

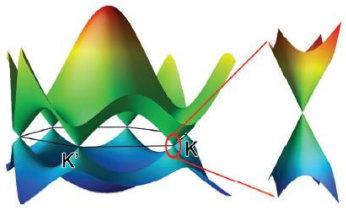

graphene

Nat. Mater. 2014, 13, 851. Science 2015, 347, 294.

Topological Dirac semimetal

Dirac Hamiltonian:

$$H = \begin{pmatrix} v\vec{\sigma}\cdot\vec{k} & 0 \\ 0 & -v\vec{\sigma}\cdot\vec{k} \end{pmatrix}$$

Weyl Hamiltonian:

$$H = \pm v\vec{\sigma}\cdot\vec{k}$$

One Dirac fermion can be viewed as two copies of Weyl fermions with opposite chirality.

Dirac semimetal
(doubly degenerated bands)

$ZrTe_5$

Na_3Bi,

Cd_3As_2

Breaking
time-reversal symmetry
or inversion symmetry

Weyl semimetal
(non-degenerated bands)

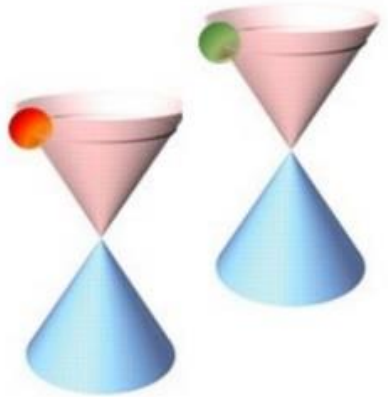

TaAs

NbAs

NbP

TaP

Topological Dirac semimetal: Cd_3As_2

Cd_3As_2 structure:

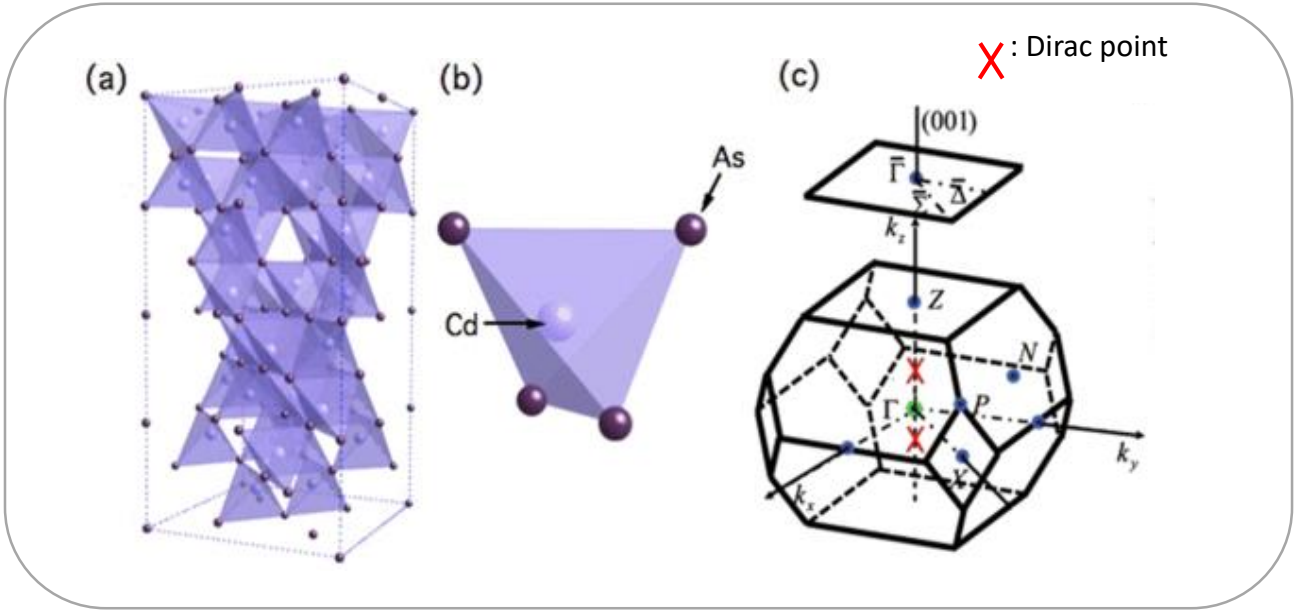

ARPES

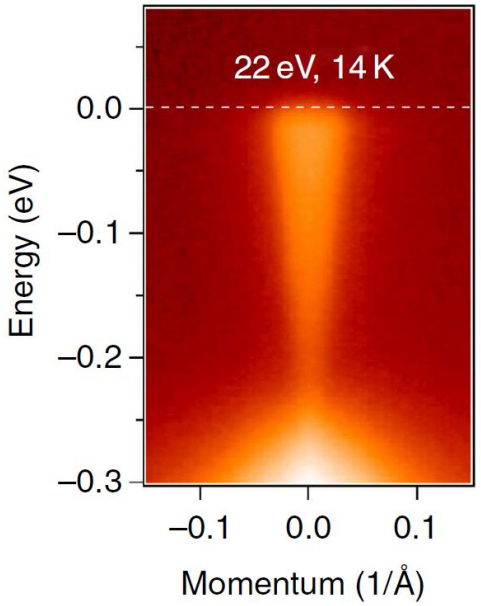

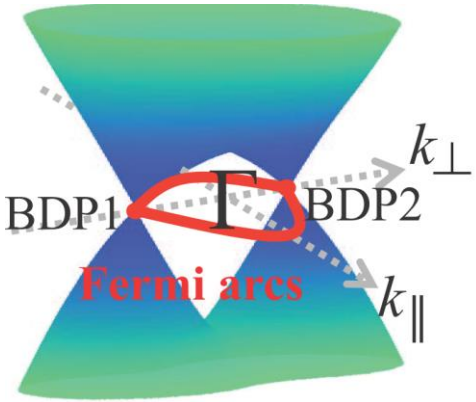

Nat. Commun. 5, 3786 (2014).

1. Synthesis and characterization of Dirac semimetal Cd_3As_2 nanostructures

CVD method:

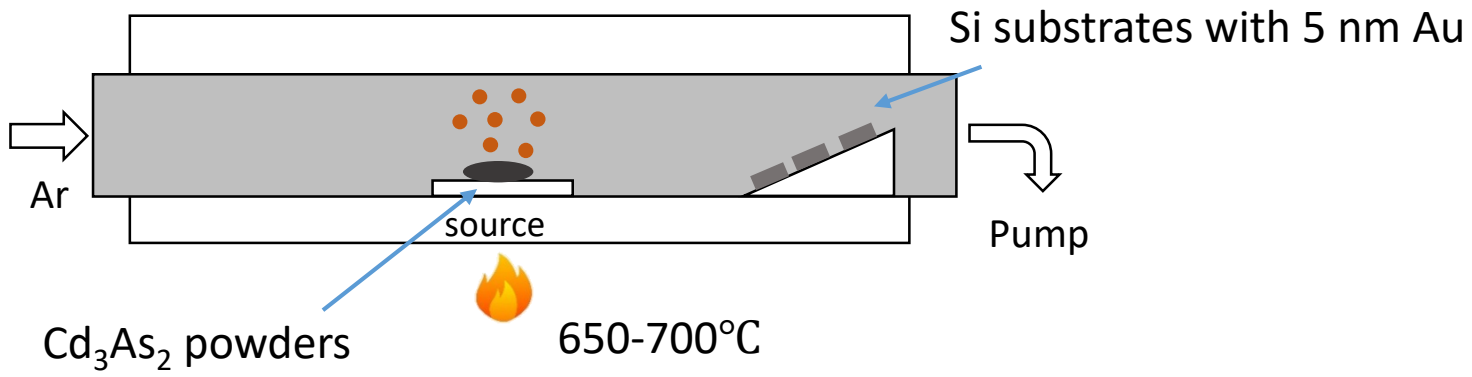

Characterization of Cd_3As_2 nanostructures

length:
~100 um
diameter:
50-500 nm

SEM

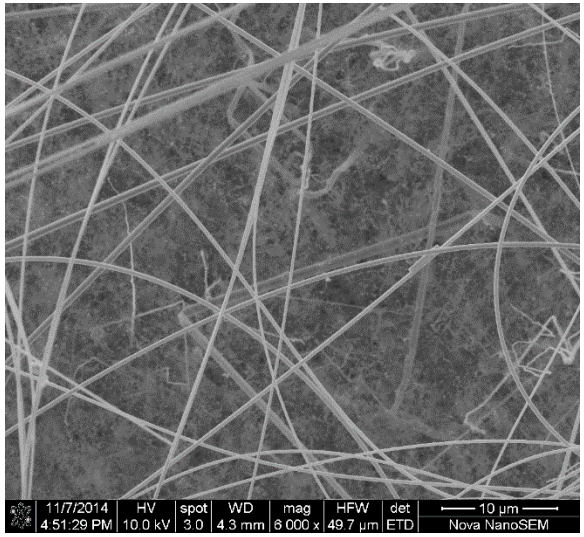

EDS

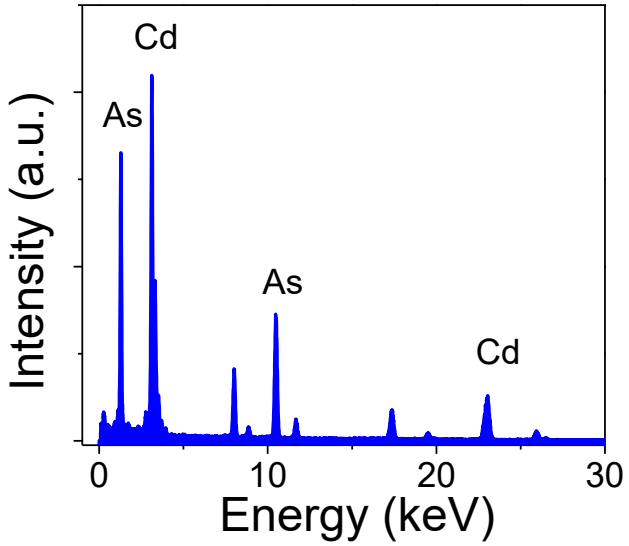

$$\frac{Cd}{As} = \frac{58.3}{41.7} \cong \frac{3}{2}$$

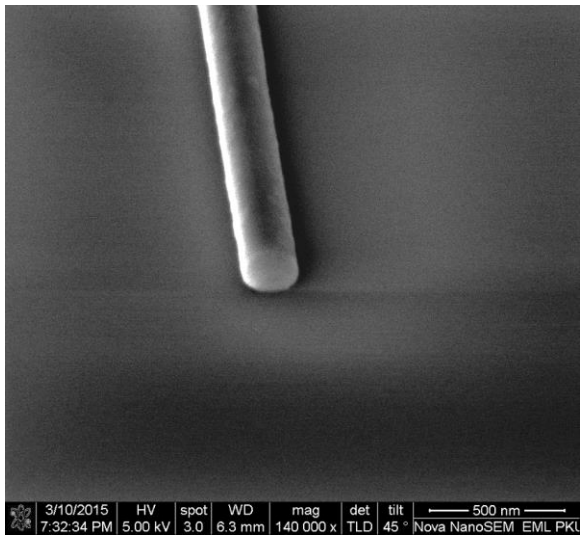

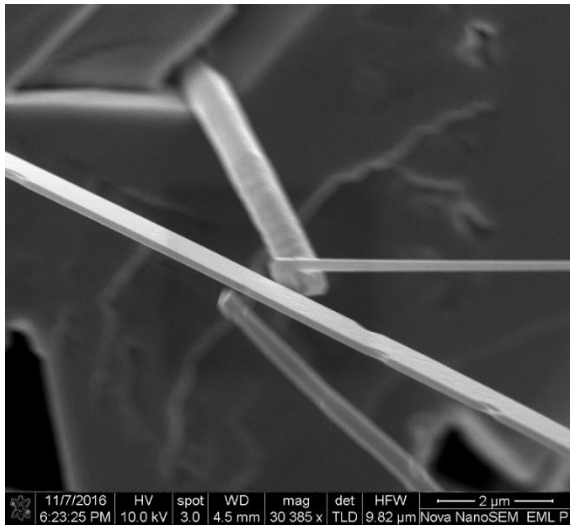

Characterization of Cd_3As_2 nanostructures

SEM

TEM

Selected area electron diffraction

[112] axis

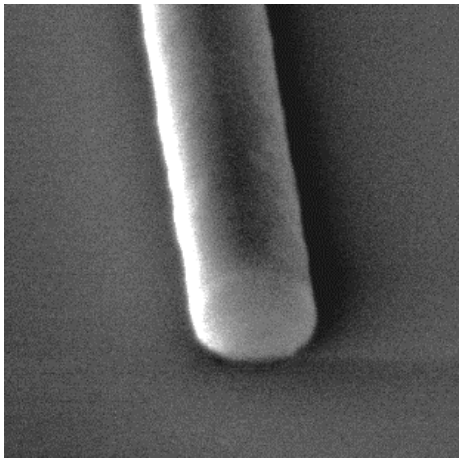

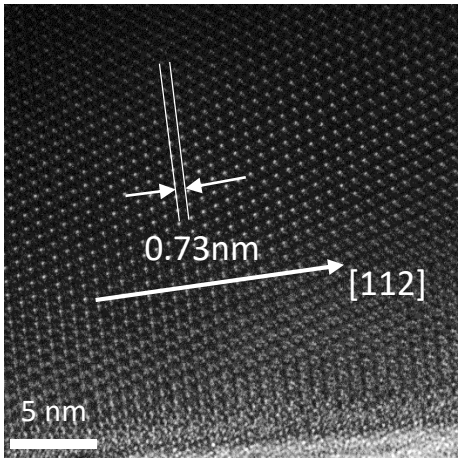

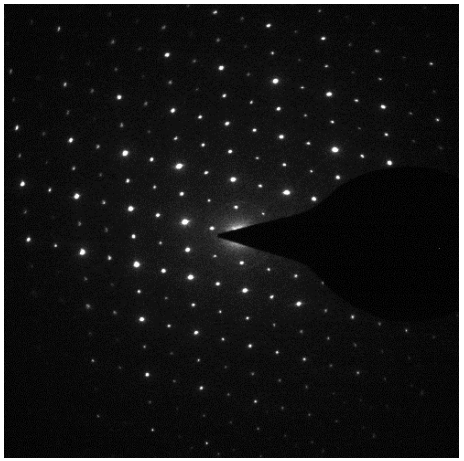

[110] axis

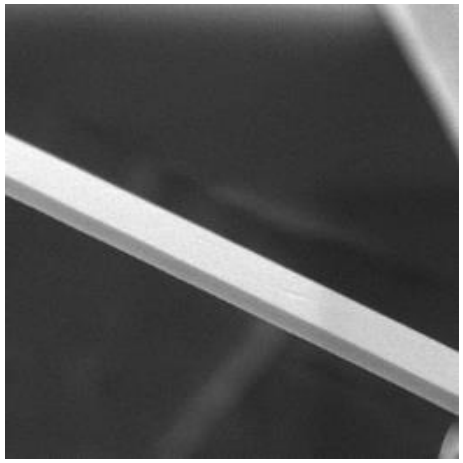

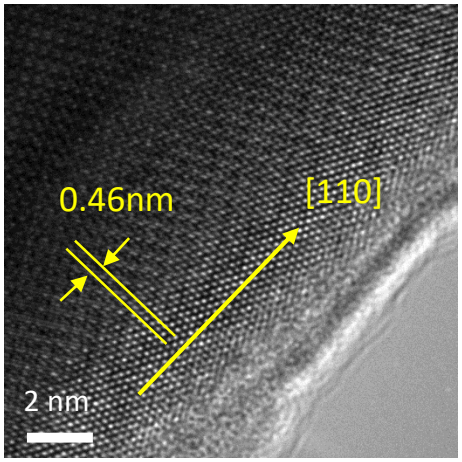

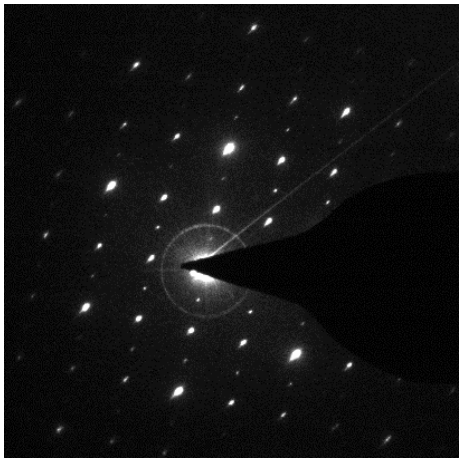

Characterization of Cd_3As_2 nanostructures

length:
~x0 um
thickness:
~x0 nm

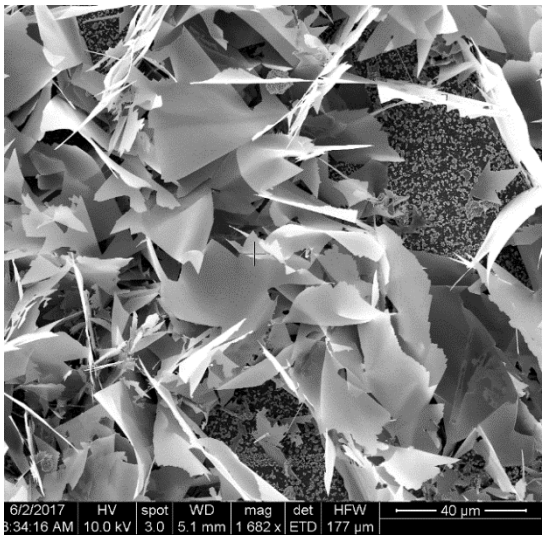

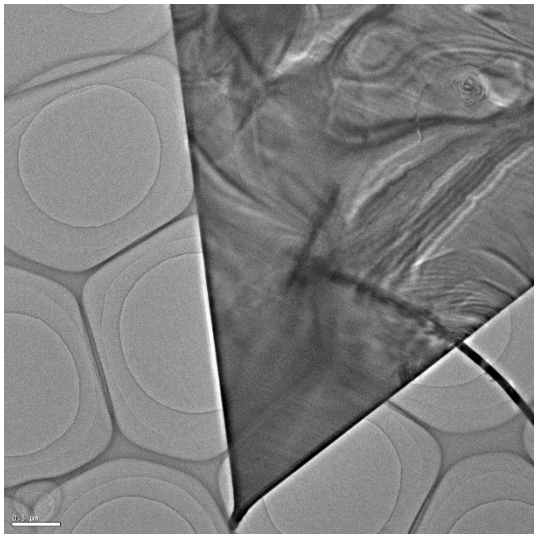

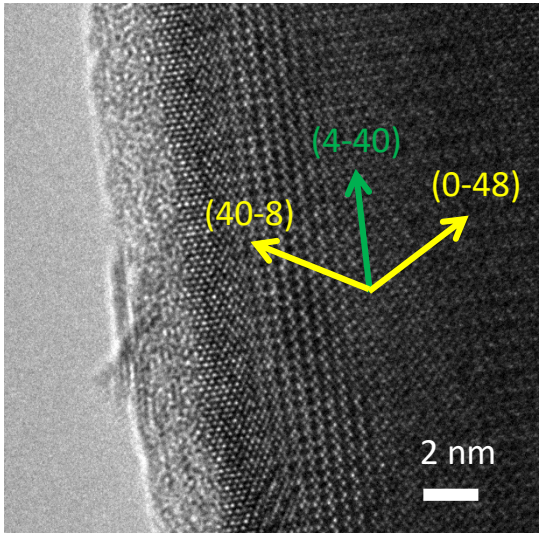

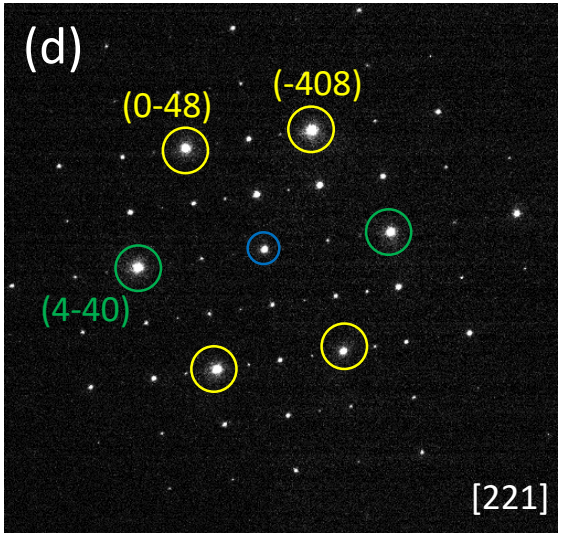

surface:

(112) surface;

edge direction:

[1-10] axis

2. Transport properties of Cd_3As_2

I. Chiral anomaly effect in Cd_3As_2 nanowires and nanoplates

II. Aharonov-Bohm oscillations in Cd_3As_2 nanowires

III. Two carrier transport in Cd_3As_2 nanoplates

Cd_3As_2 device

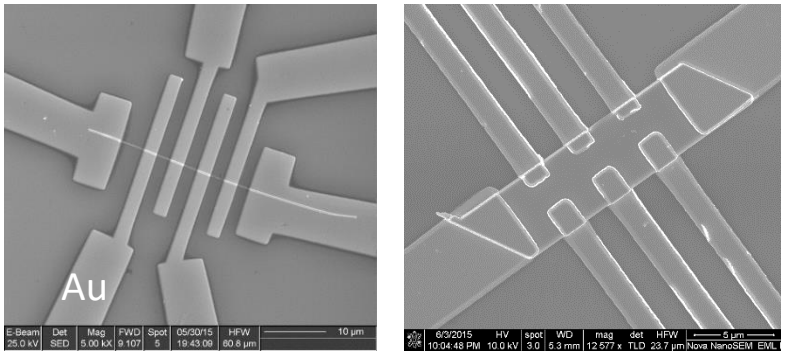

2. Transport properties of Cd_3As_2

I. Chiral anomaly effect in Cd_3As_2 nanowires and nanoplates

II. Aharonov-Bohm oscillations in Cd_3As_2 nanowires

III. Two carrier transport in Cd_3As_2 nanoplates

Cd_3As_2 device

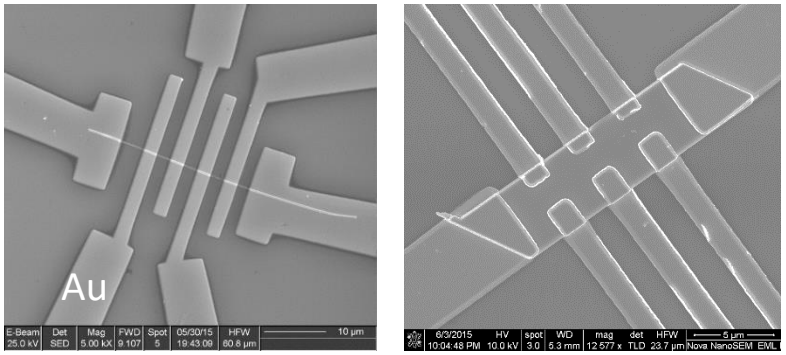

Chiral anomaly effect

Weyl fermion: chirality

$$\chi = \frac{\vec{\sigma} \cdot \vec{p}}{|\vec{p}|}$$

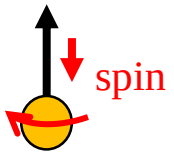

Left handed

Right handed

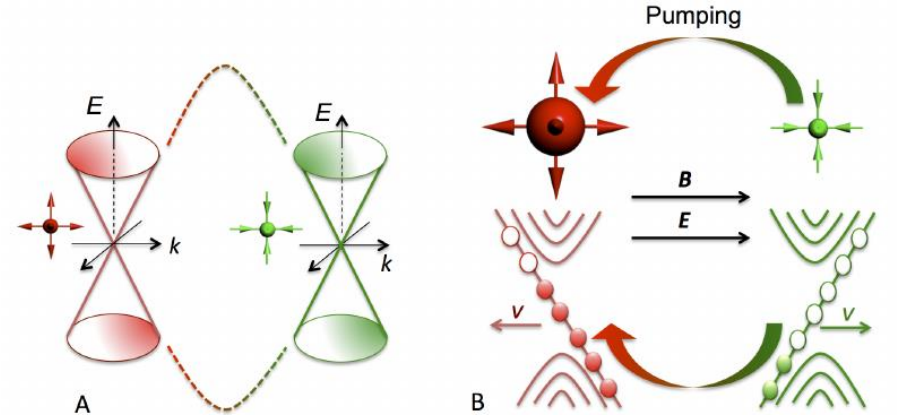

$$\partial_\mu j_\chi^\mu = -\chi \frac{e^3}{4\pi^2\hbar^2} \boldsymbol{E} \cdot \boldsymbol{B}$$

$$J_C = \left(\frac{e}{h}\right)^2 (\mu_L - \mu_R) B$$

In the transport measurements:

negative magnetoresistance (MR)

Negative magnetoresistance

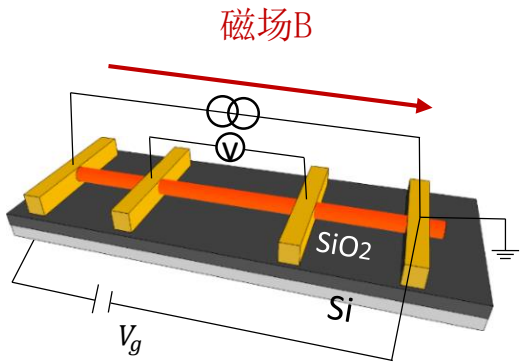

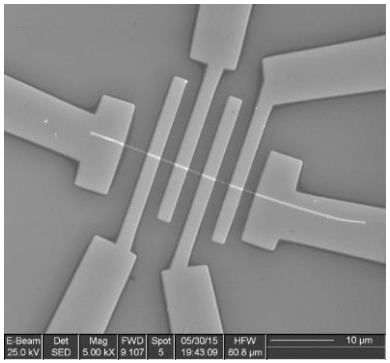

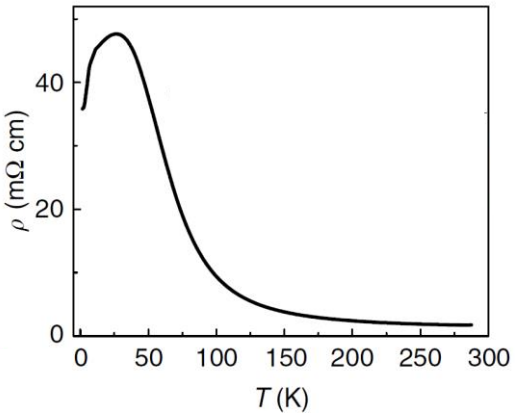

Angular-dependence of MR:

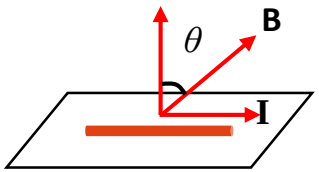

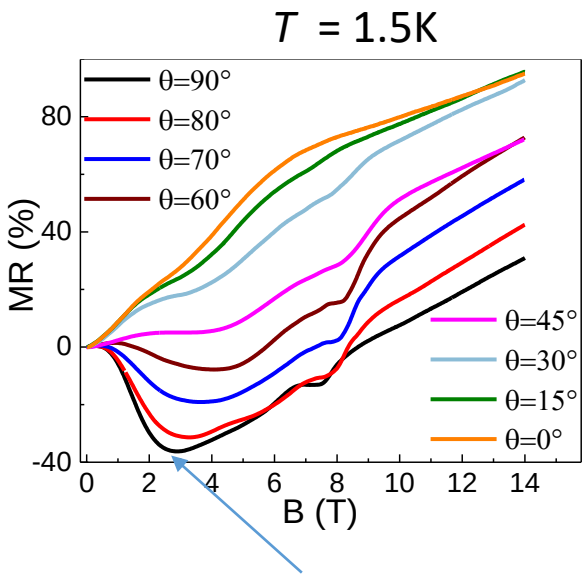

Cai-Zhen Li †, Li-Xian Wang† *et al.* ***Nat. Commun.*** 6, 10137 (2015).

Negative magnetoresistance

Temperature-dependence of negative MR :

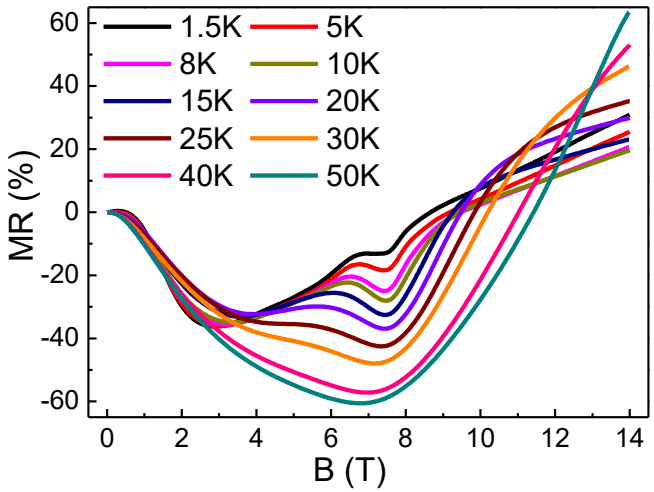

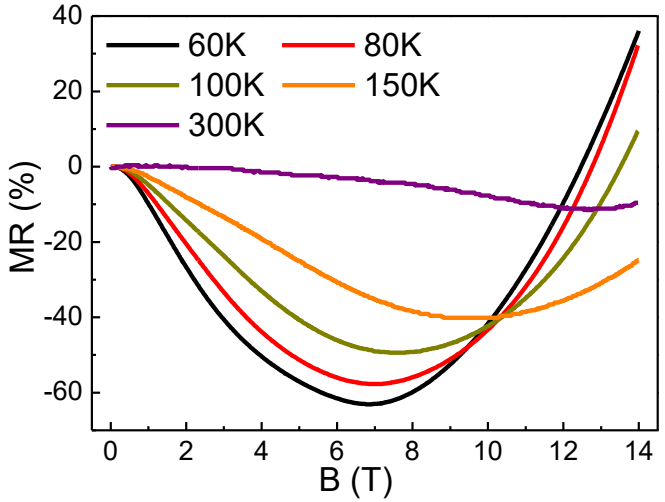

Gate tunable negative MR :

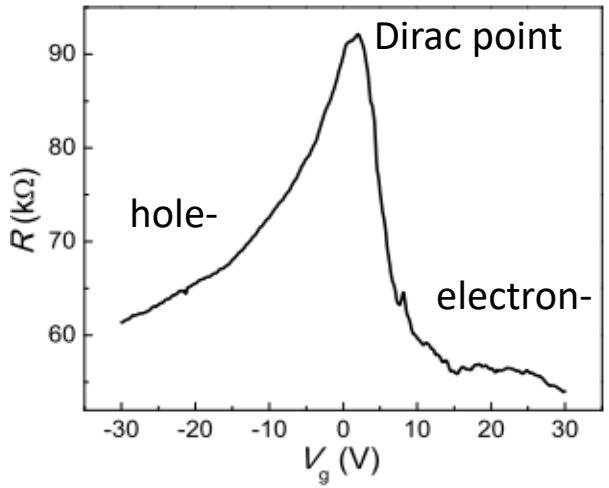

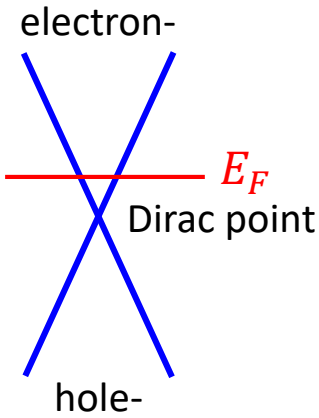

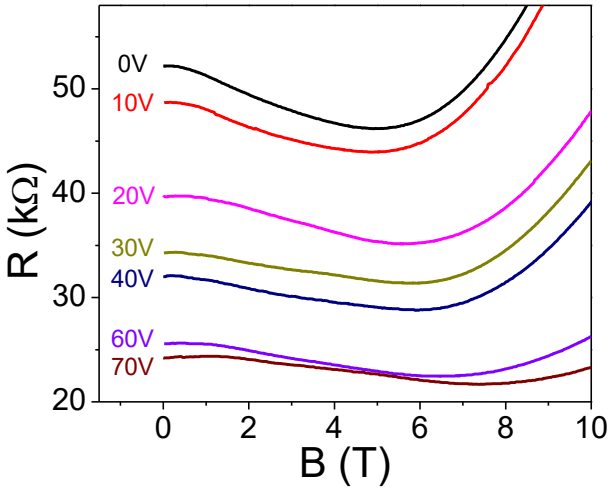

Low carrier concentration $n \sim 10^{17}/cm^3$ (V_g=0 V)

Negative magnetoresistance

nanowire

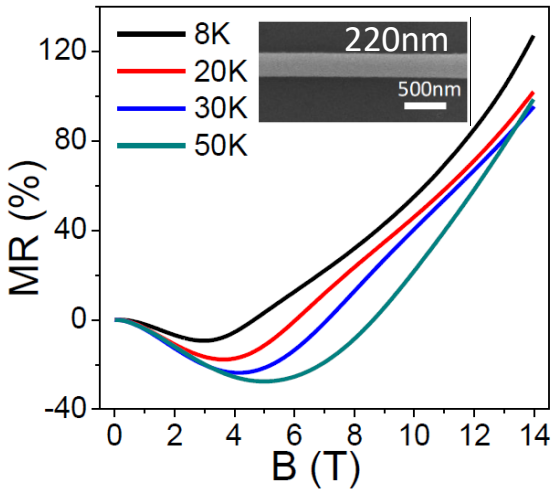

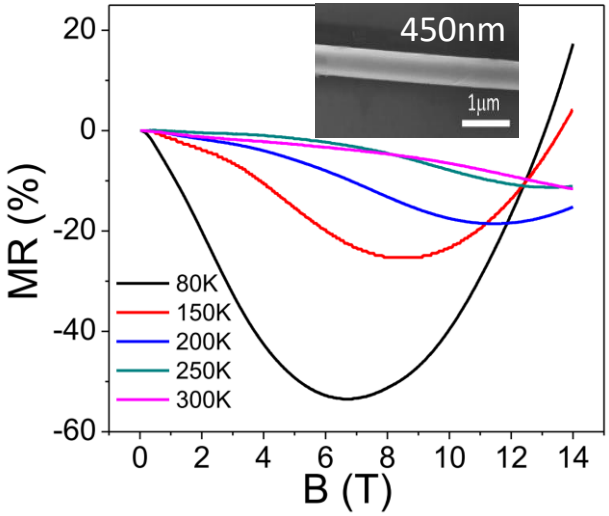

nanoplate

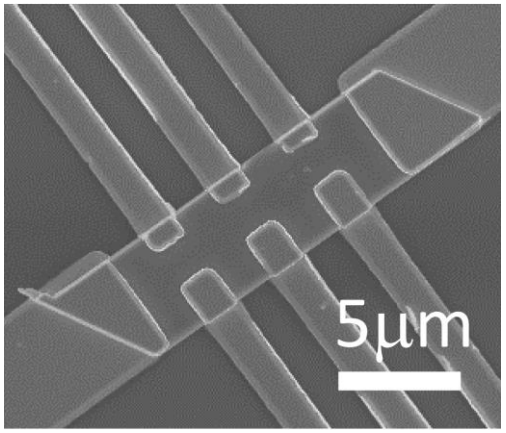

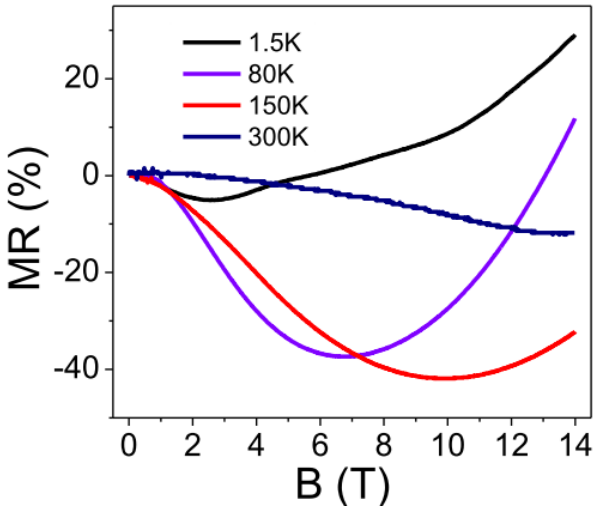

The negative MR can be observed in all nanowires devices with different diameters, as well as in nanoplate devices, indicating that the negative MR is independent of the geometry or size of the sample, and is an intrinsic property of the material.

Negative magnetoresistance

Negative MR in other materials:

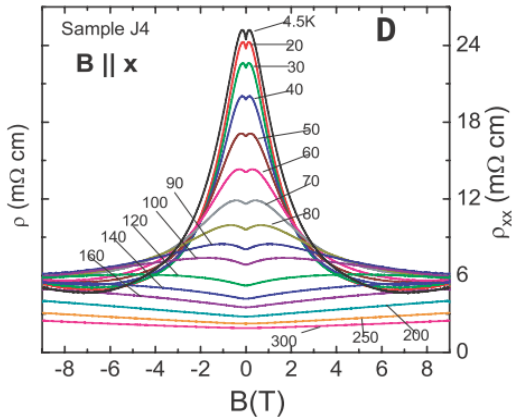

Na_3Bi *Science*. **350**.413 (2015)

Princeton, Ong group

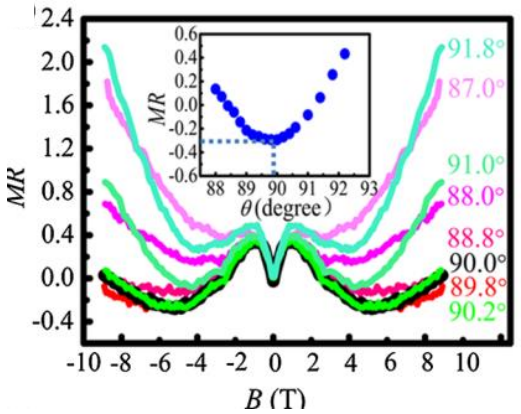

TaAs *Phys. Rev. X* **5**, 031023 (2015)

Chinese Academy of Sciences

Genfu Chen Group

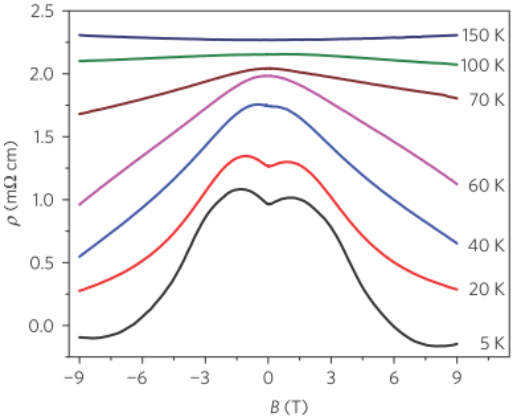

$ZrTe_5$ *Nat.Phys.* 12,550 (2016)

Brookhaven National Lab, Valla Group

Our work (highly cited paper):

1

Giant negative magnetoresistance induced by the chiral anomaly in individual Cd3As2 nanowires

Li, CZ; Wang, LX; (...); Yu, DP

Dec 2015 | NATURE COMMUNICATIONS 6

Dirac electronic materials beyond graphene and topological insulators have recently attracted considerable attention. Cd3As2 is a Dirac semimetal with linear dispersion along all three momentum directions and can be viewed as a three-dimensional analogue of graphene. By breaking of either time-reversal symmetry or spatial inversion symmetry, the Dirac semimetal is believed to transform into a W ... Show more

get it BIT Free Full Text from Publisher View Full Text on ProQuest •••

342 Citations

33 References

Related records

2. Transport properties of Cd_3As_2

I. Chiral anomaly effect in Cd_3As_2 nanowires and nanoplates

II. Aharonov-Bohm oscillations in Cd_3As_2 nanowires

III. Two carrier transport in Cd_3As_2 nanoplates

Cd_3As_2 device

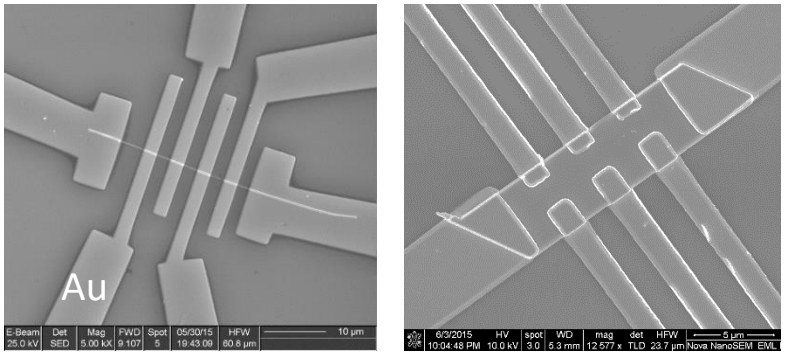

Aharonov-Bohm oscillations

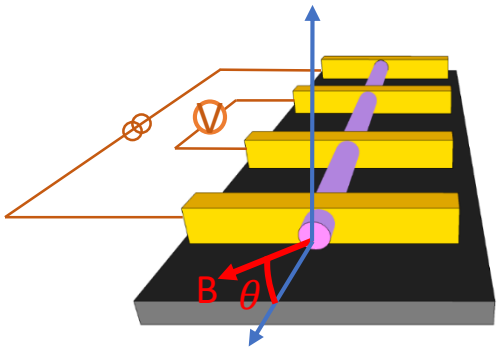

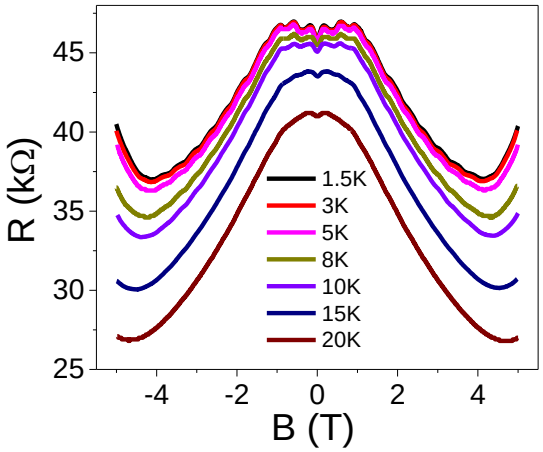

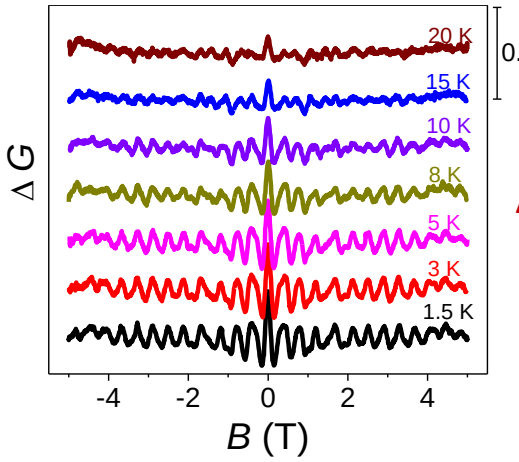

Period:

$\Delta B = 0.38T$

Flux

$\Phi \sim h/e$

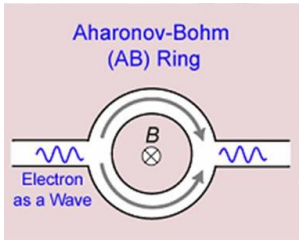

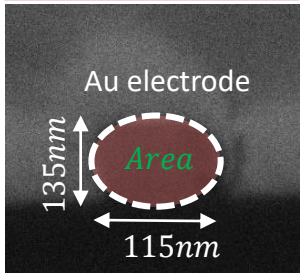

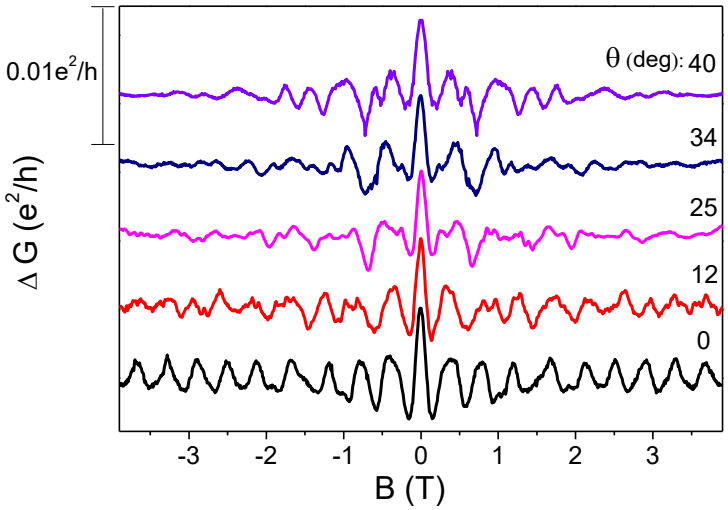

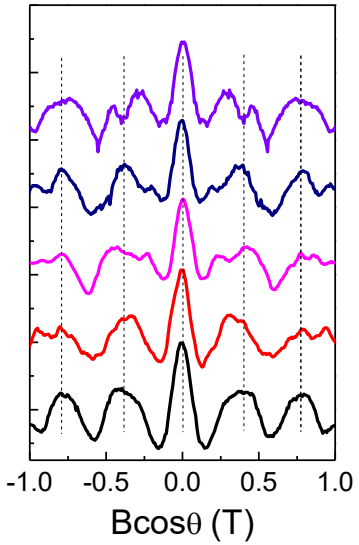

Li-Xian Wang[†], **Cai-Zhen Li**[†] *et al.*, *Nat Commun* 7, 10769 (2016).

Aharonov-Bohm oscillations

Surface-band splitting due to **quantum confinement**:

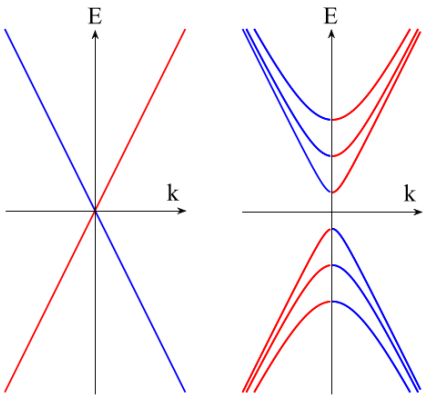

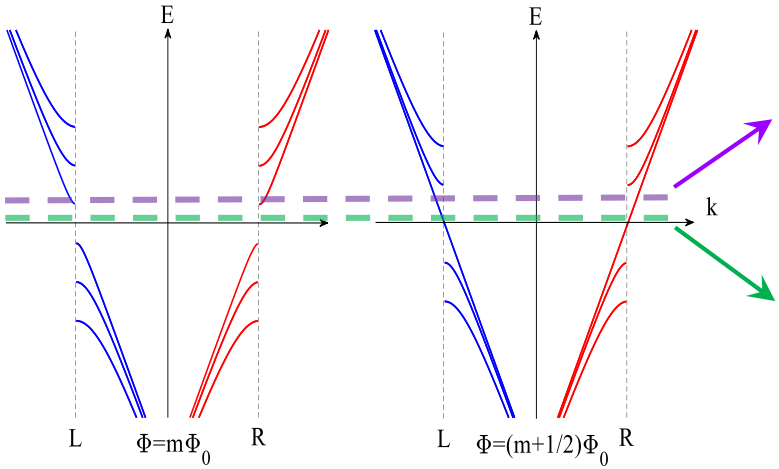

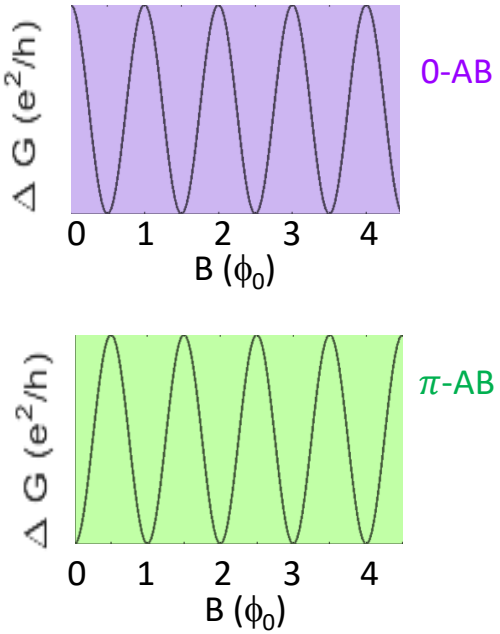

$$E = \pm\hbar v_f \sqrt{\frac{k_\parallel^2}{4\pi^2} + \left(\frac{m + \frac{1}{2} - \frac{\Phi}{\Phi_0}}{C}\right)^2}$$

in which, C is perimeter, $m = 0, \pm1, \pm2, \ldots$

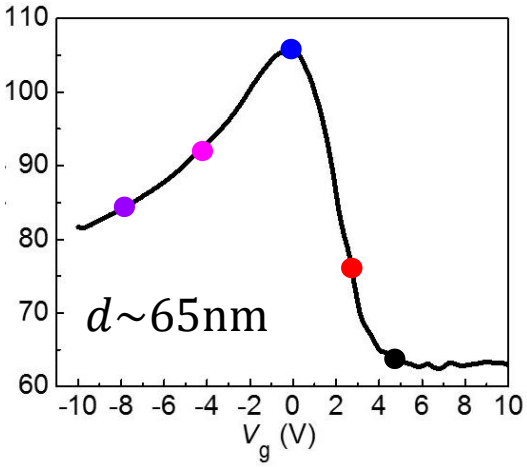

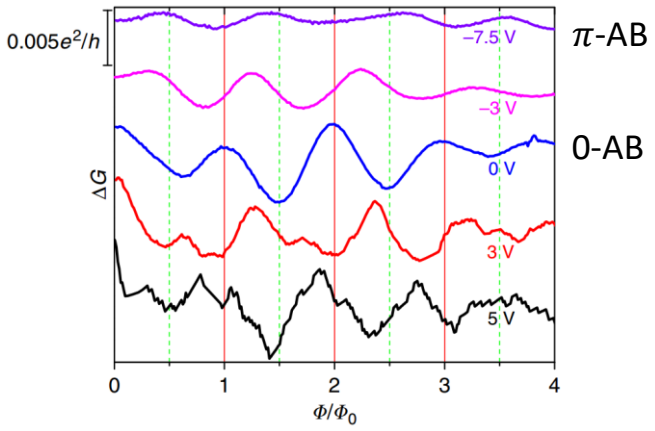

Transport Properties of Cd_3As_2

Altshuler-Aronov-Spivak effect:

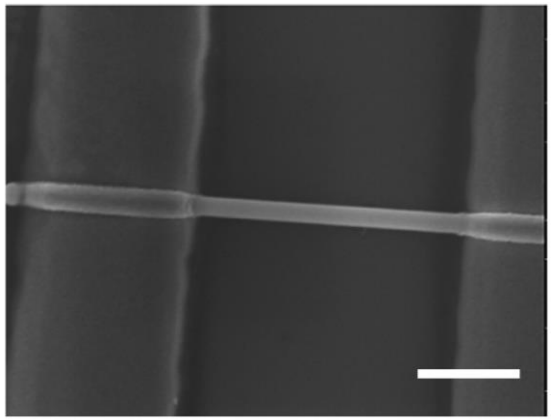

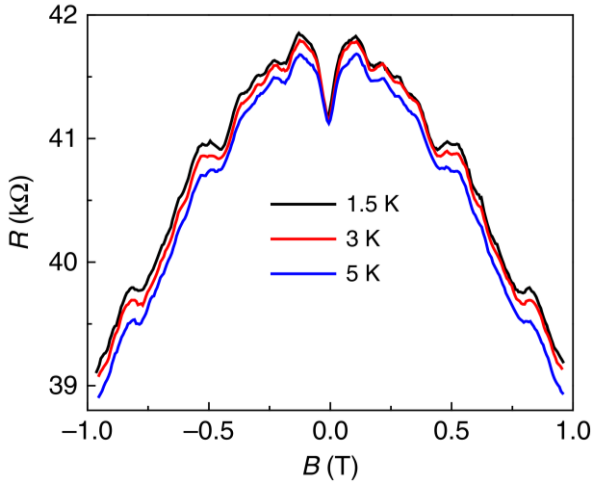

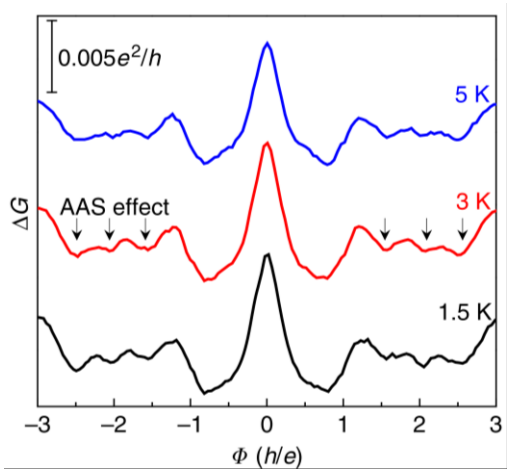

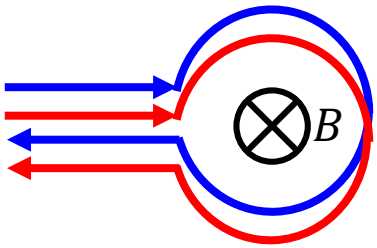

- ✓ diameter: ~200 nm
- ✓ AAS oscillations: $h/2e$
- ✓ diffusive transport around the perimeter

2. Transport properties of Cd_3As_2

I. Chiral anomaly effect in Cd_3As_2 nanowires and nanoplates

II. Aharonov-Bohm oscillations in Cd_3As_2 nanowires

III. Two carrier transport in Cd_3As_2 nanoplates

Cd_3As_2 device

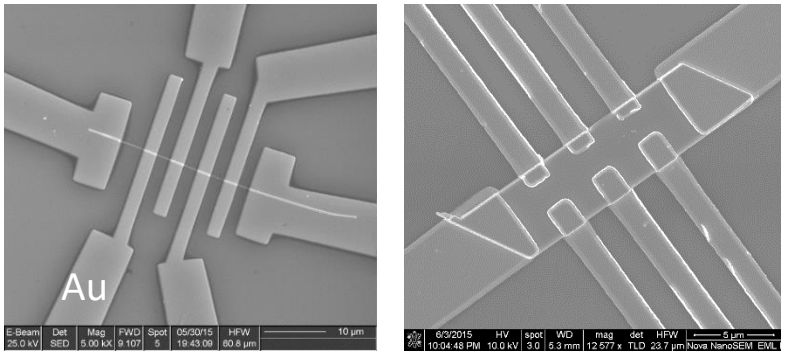

Two carrier transport in Cd_3As_2 nanoplates

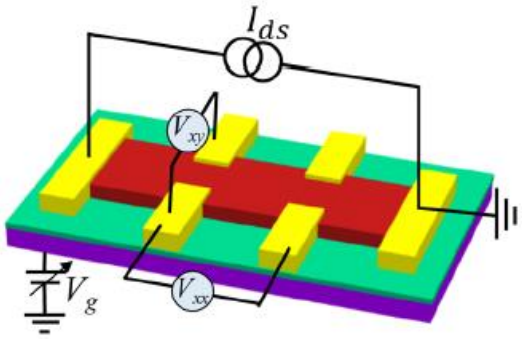

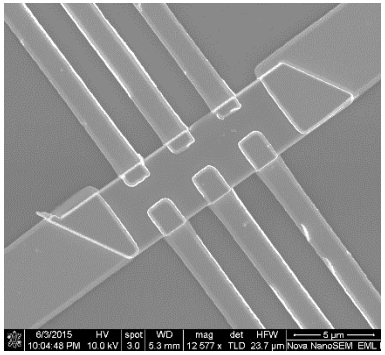

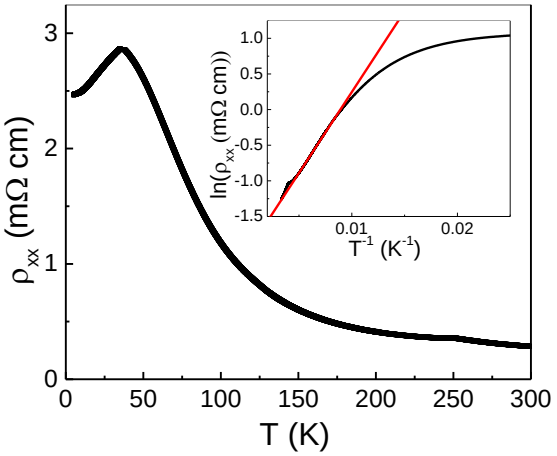

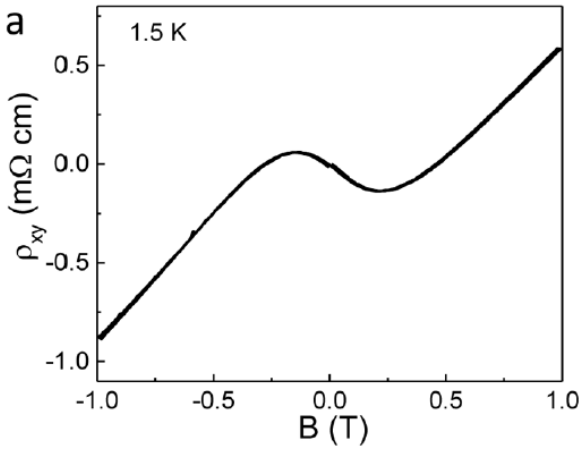

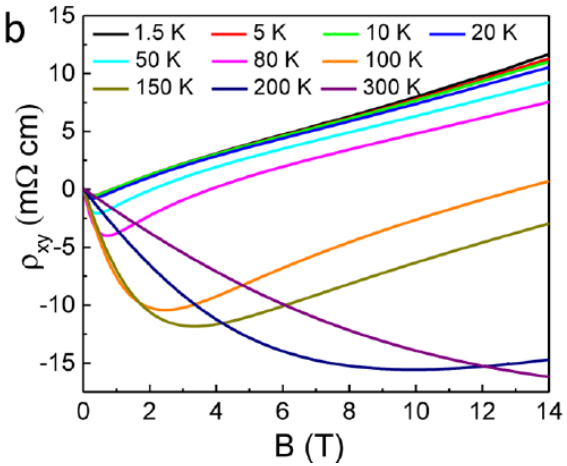

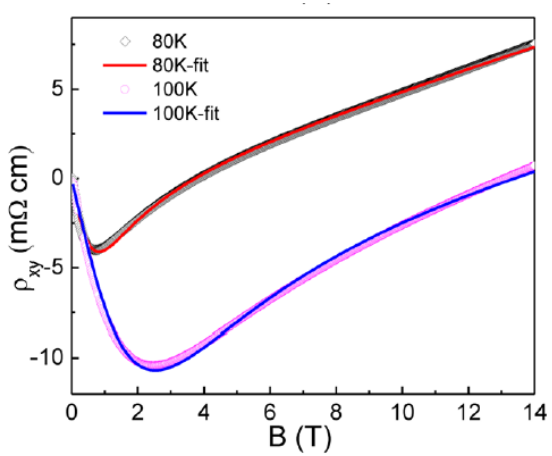

Two-carrier model: $$\rho_{xy} = \frac{1}{e}\frac{(n_h\mu_h^2 - n_e\mu_e^2) + \mu_h^2\mu_e^2B^2(n_h - n_e)}{(n_h\mu_h + n_e\mu_e)^2 + \mu_h^2\mu_e^2B^2(n_h - n_e)^2}B$$

$n \sim 10^{17}/cm^3$

Two carrier transport in Cd_3As_2 nanoplates

Gate tunable two-carrier transport:

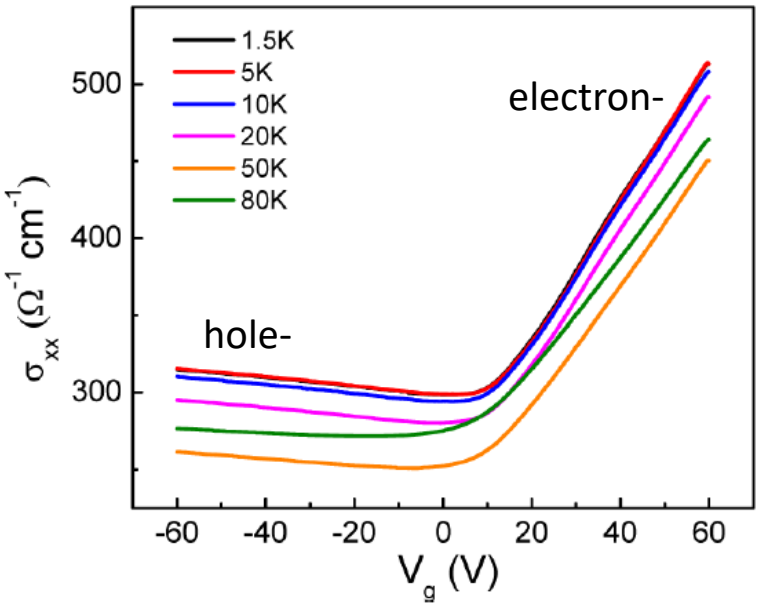

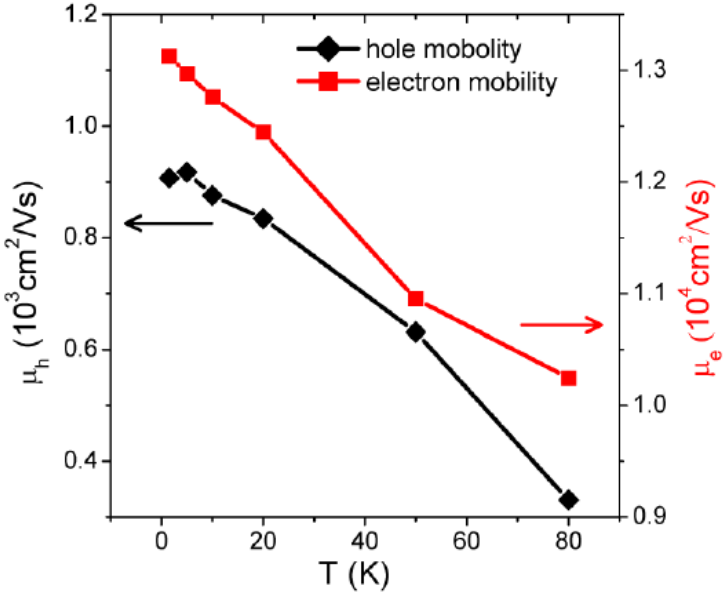

mobility:

$\mu_e \sim 1 \times 10^4 cm^2/Vs$

$\mu_h \sim (0.4 - 0.9) \times 10^3 cm^2/Vs$

Research contents

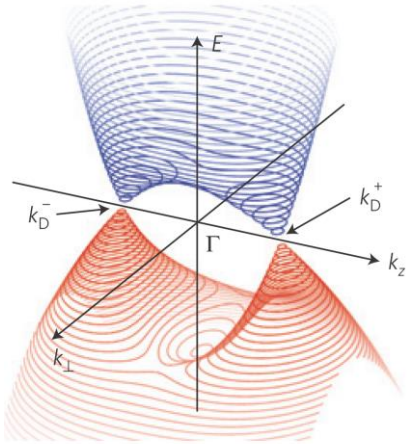

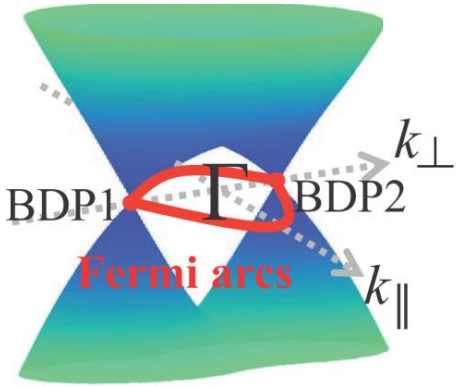

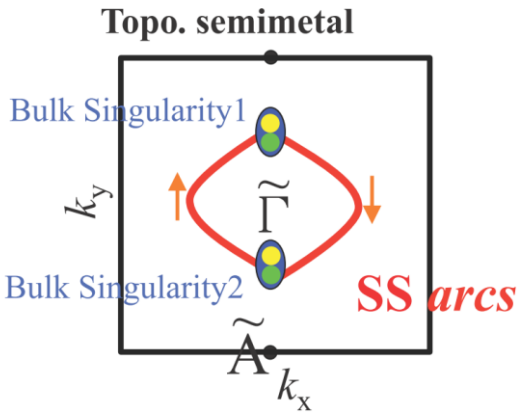

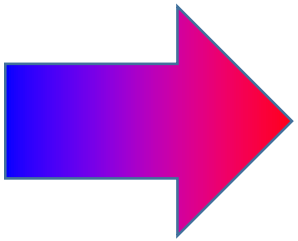

Topological physics of Dirac fermions and Fermi arc surface states

Low-power electronic devices

Topological superconductivity

3. Transport properties in Cd_3As_2 based Josephson junctions

I. Gate-tunable topological superconductivity and 4π-periodic supercurrent (in Cd_2As_2 nanowires)

II. Fermi-arc supercurrent oscillations (in Cd_3As_2 nanoplates)

III. Higher order topological hinge states (in Cd_3As_2 nanoplates)

Nb-Cd_3As_2-Nb Josephson junctions

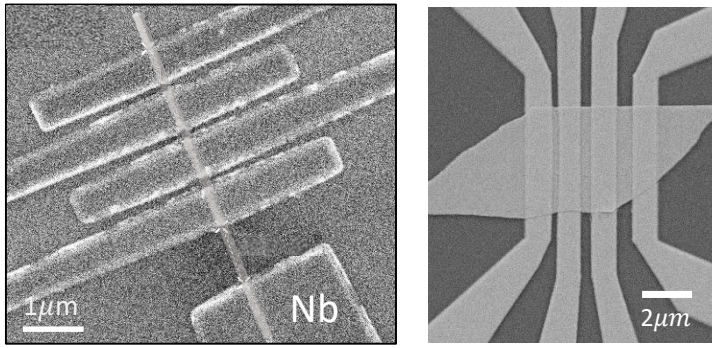

3. Transport properties in Cd_3As_2 based Josephson junctions

I. Gate-tunable topological superconductivity and 4π-periodic supercurrent (in Cd_2As_2 nanowires)

II. Fermi-arc supercurrent oscillations (in Cd_3As_2 nanoplates)

III. Higher order topological hinge states (in Cd_3As_2 nanoplates)

Nb-Cd_3As_2-Nb Josephson junctions

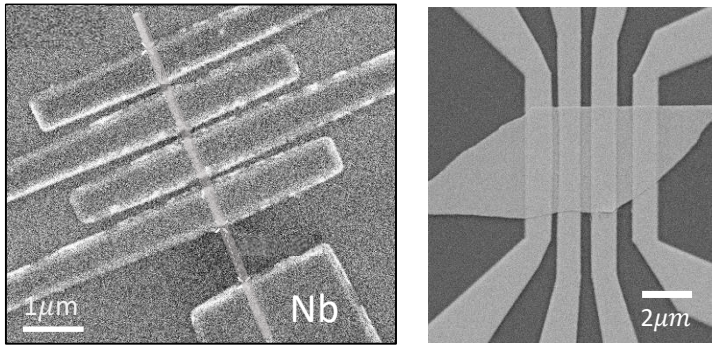

Josephson junctions

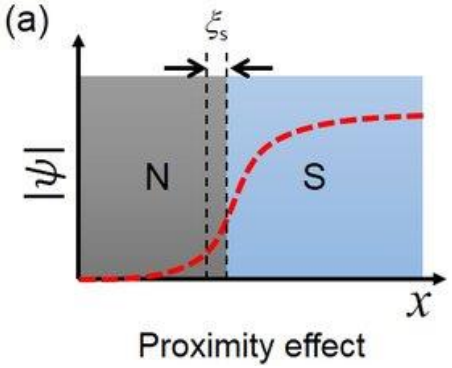

Proximity effect

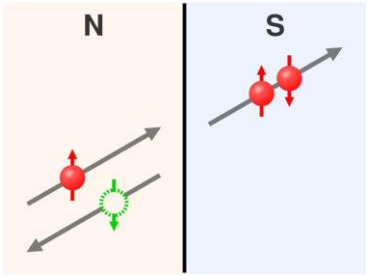

Andreev reflection

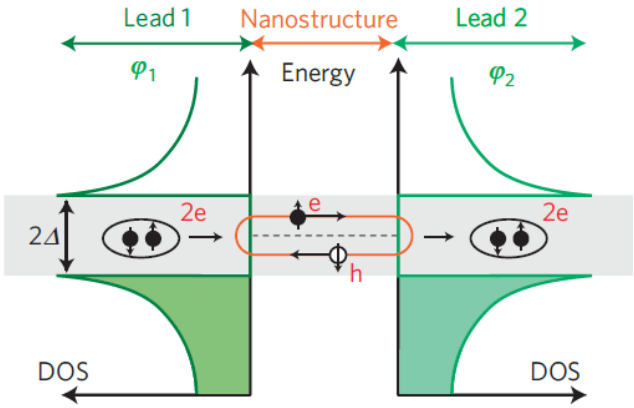

Andreev bound states

Josephson junction

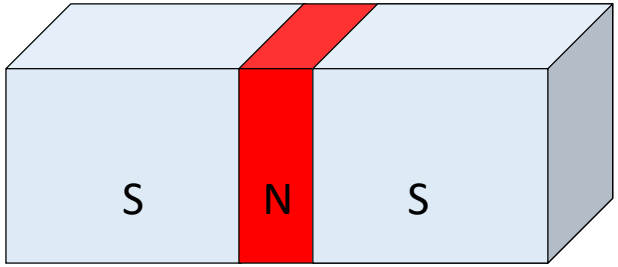

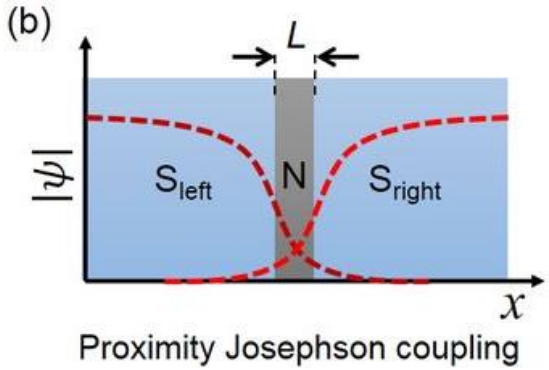

Proximity Josephson coupling

Order parameter: $\Delta_{1,2} = |\Delta_{1,2}| e^{i\varphi_{1,2}}$

Phase difference: $\varphi = \varphi_1 - \varphi_2$

$I_s = I_c \sin(\varphi)$ d.c. Josephson effect

$\frac{\partial \varphi}{dt} = \frac{2eV}{\hbar}$ a.c. Josephson effect

Under magnetic field:

$$I_c(B) = I_{c0} \left| \frac{\sin(\frac{\pi \Phi}{\Phi_0})}{\frac{\pi \Phi}{\Phi_0}} \right|$$

Gate control of AB and AAS interference

Normal state transport at T=10 K

d~64 nm

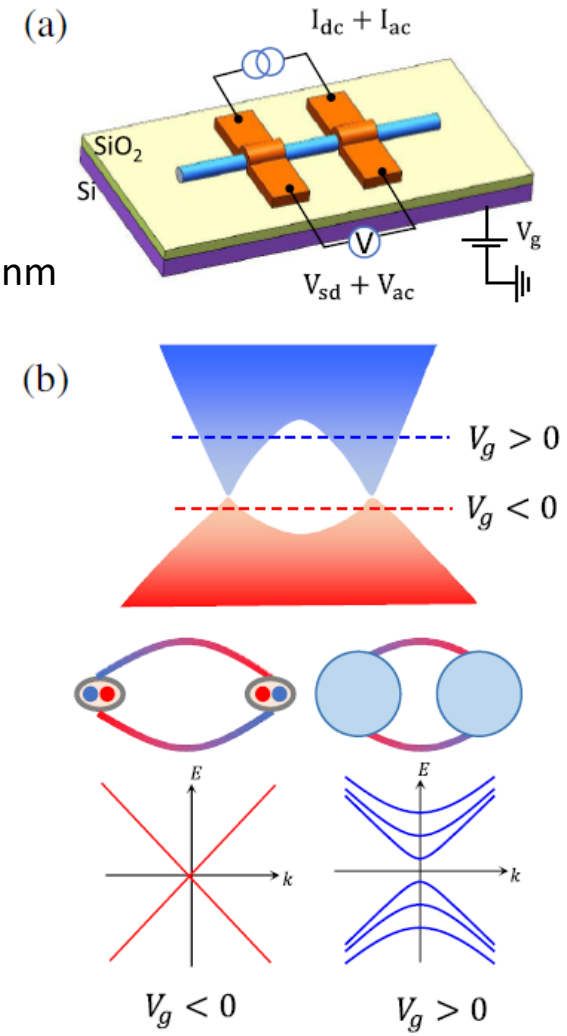

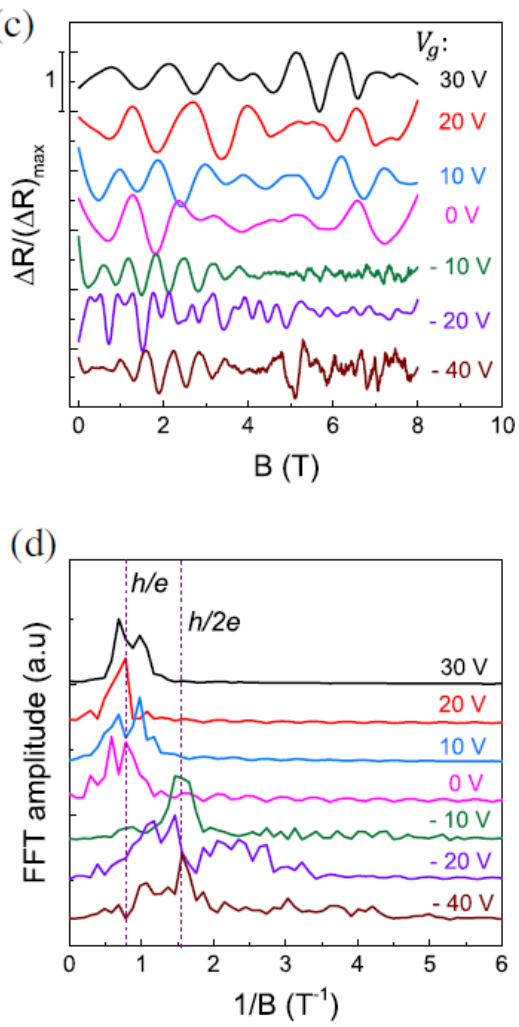

Nb-Cd_3As_2 nanowire-Nb

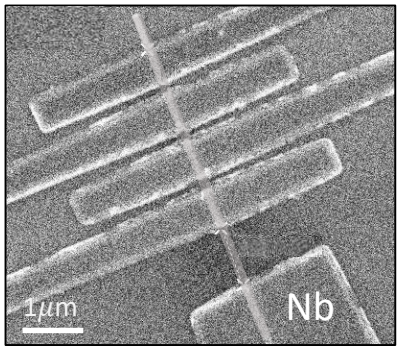

AB oscillations: h/e

AAS oscillations: $h/2e$

Cai-Zhen Li †, An-Qi Wang† *et al.* ***Phys. Rev. Lett.*** 126, 027001 (2021).

Proximity-induced supercurrent in Cd_3As_2 nanowires

T = 10 mK

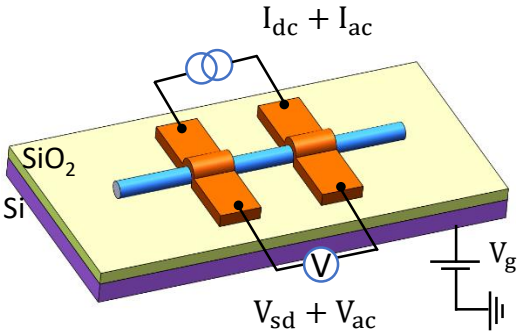

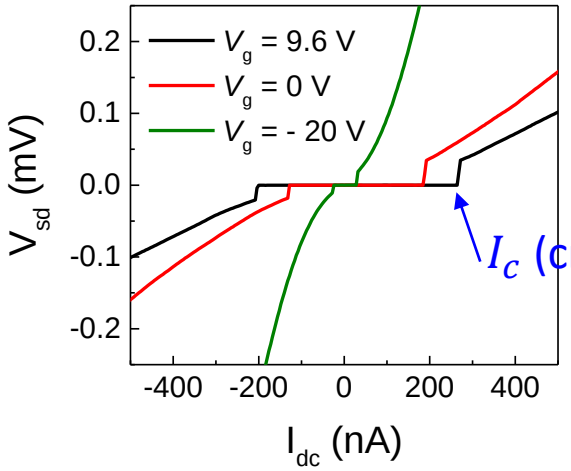

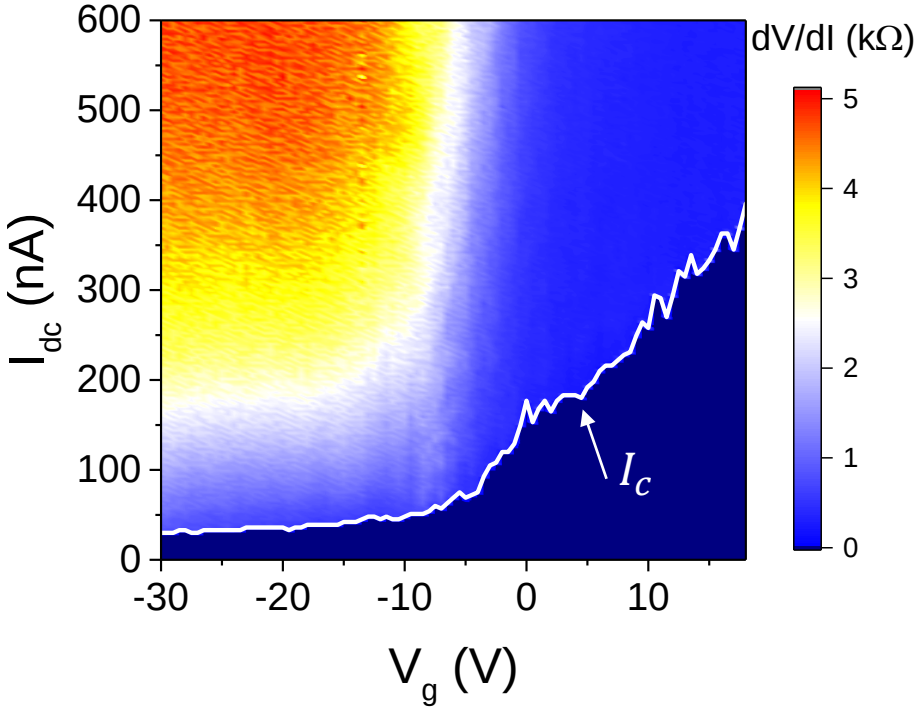

Gate-tunable I_c

Quantized orbit interference induced supercurrent oscillations

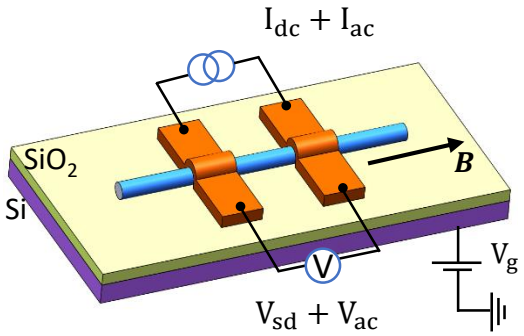

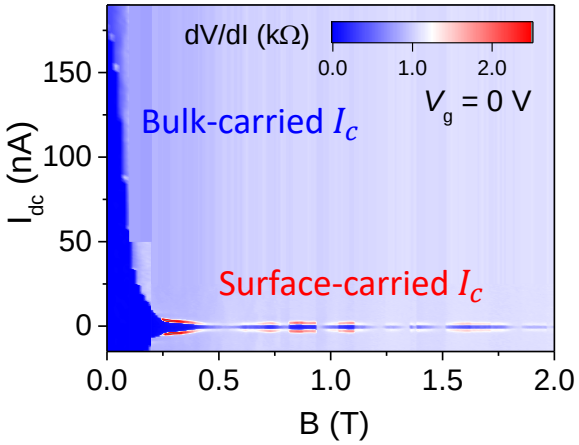

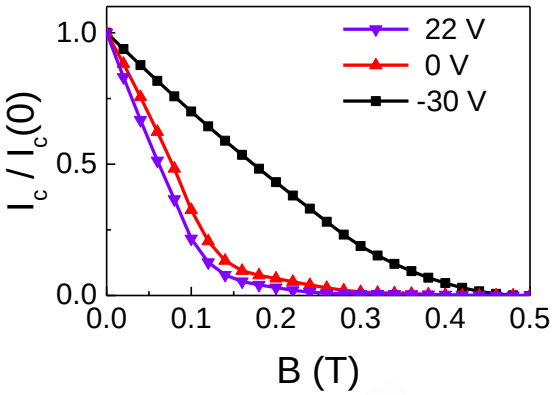

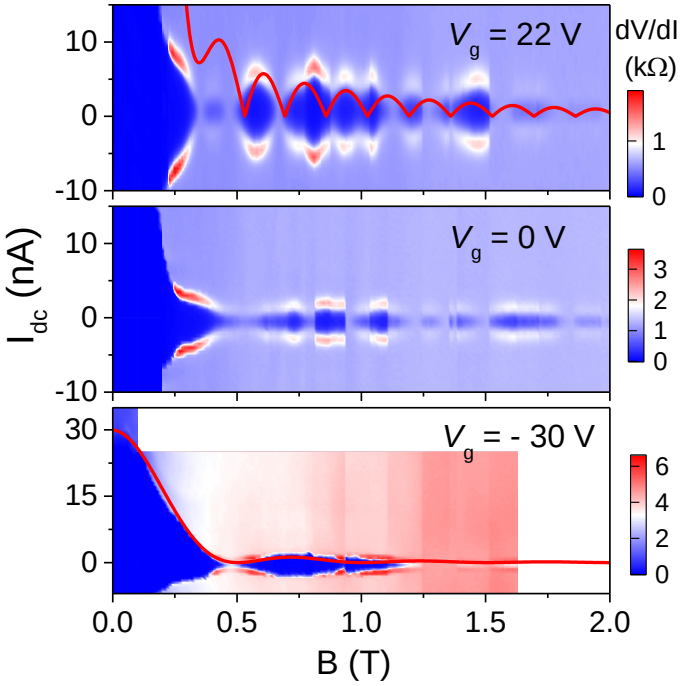

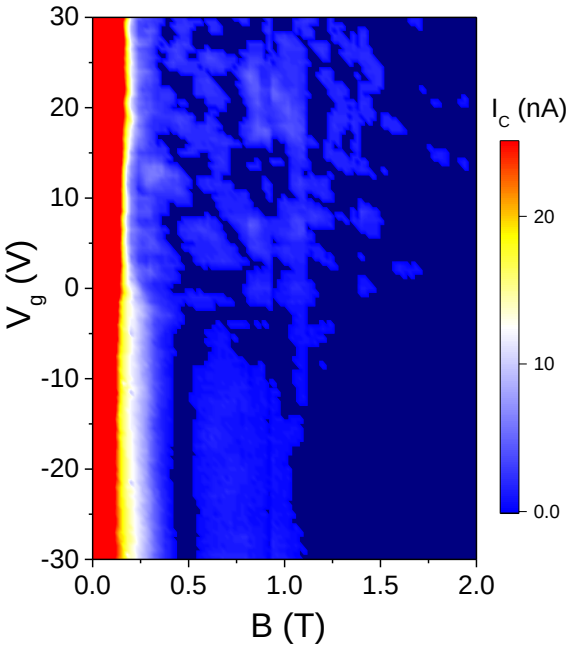

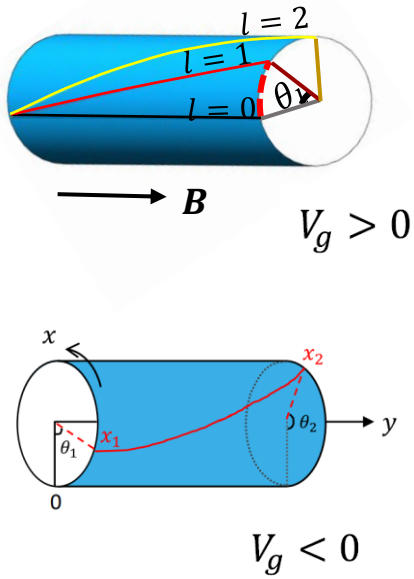

Gate control of topological phase transition

Applying a magnetic field to suppress the bulk-carried supercurrent

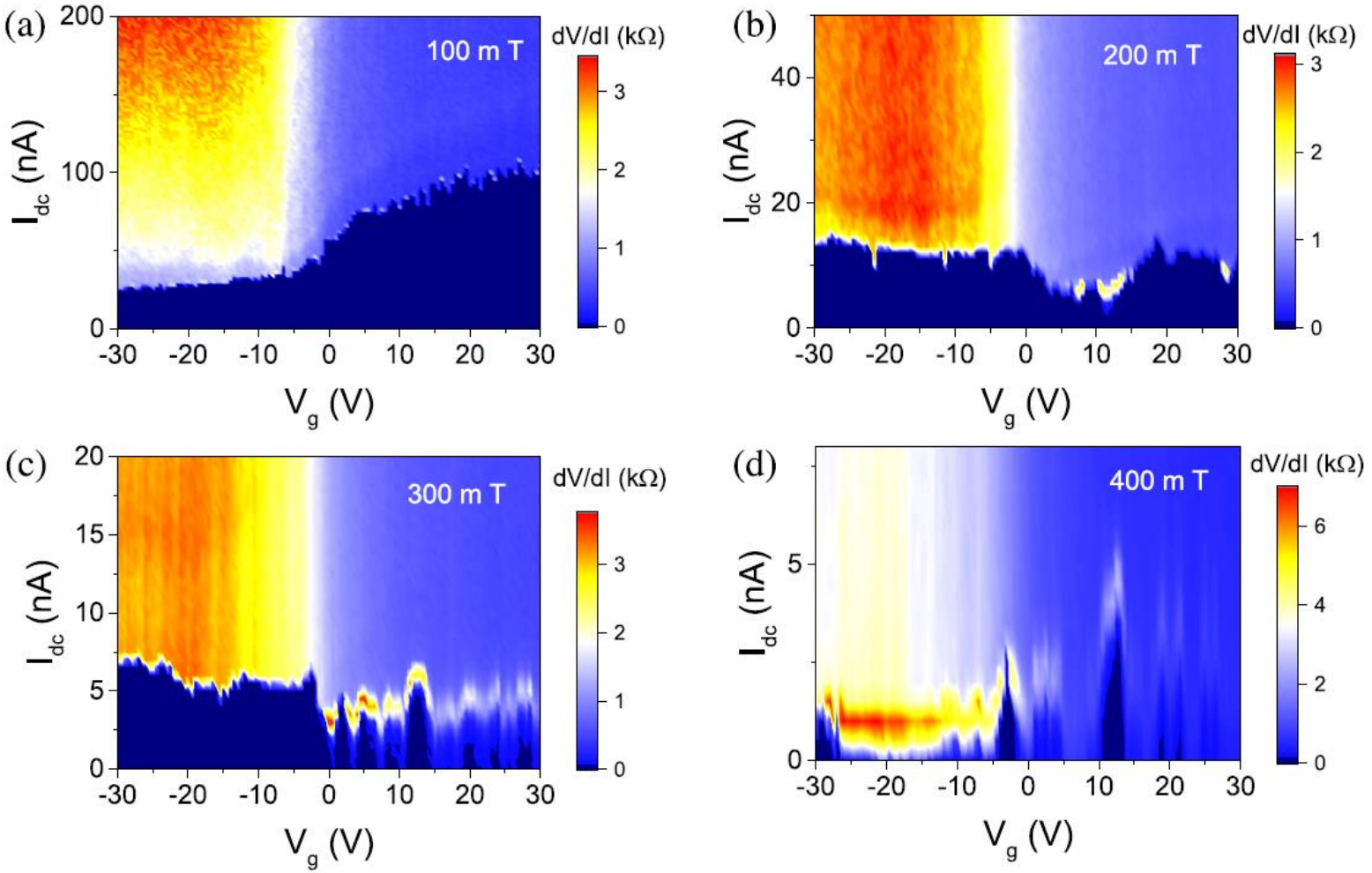

Topological protection enhance critical magnetic field B_c

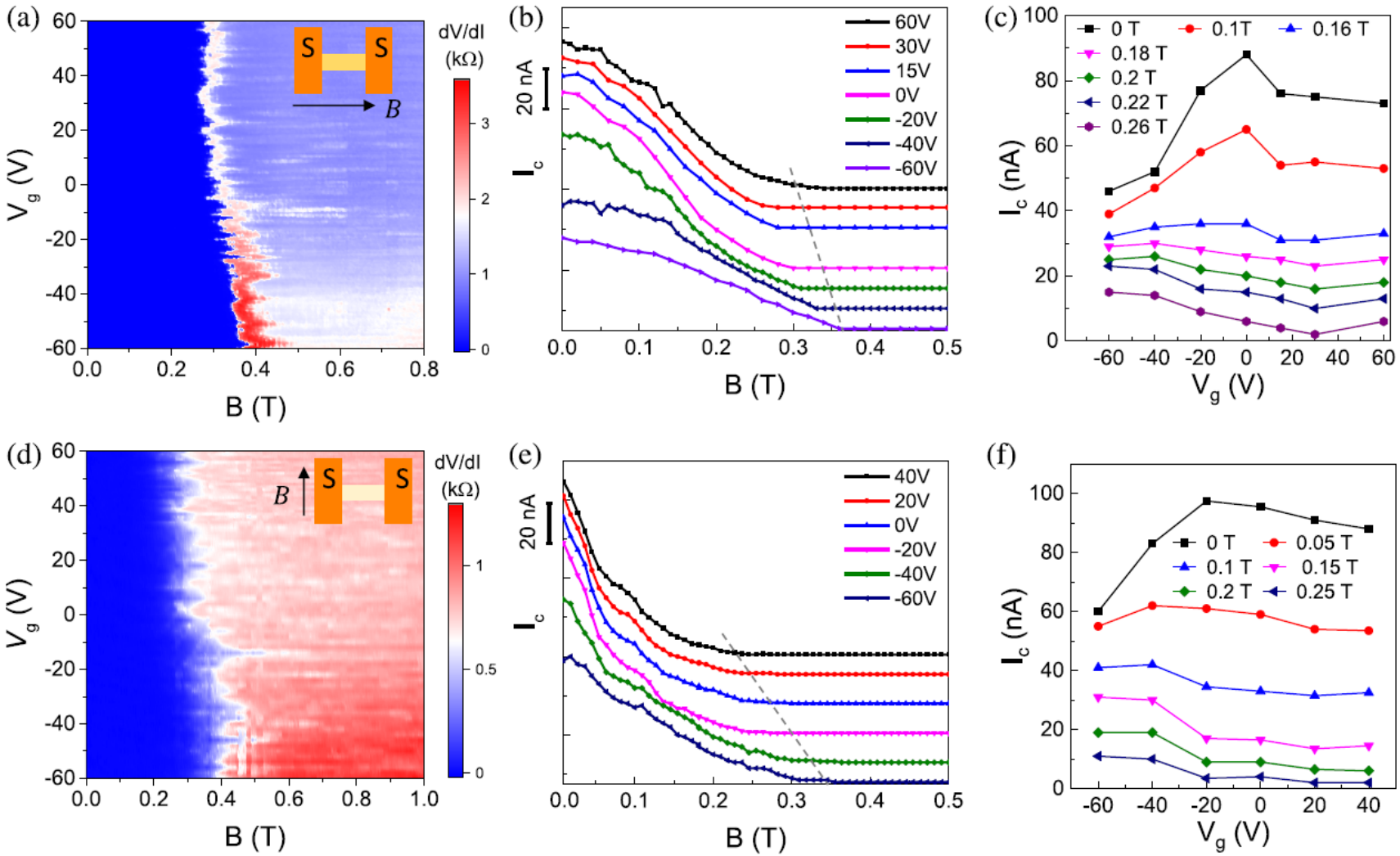

RF irradiation and 2π-periodic supercurrent

- **Conventional proximity effect**

Andreev bound states

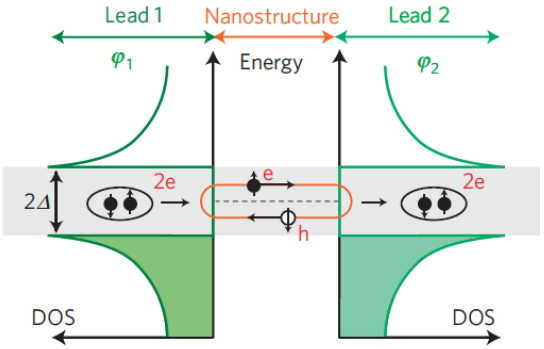

Nat. Phys. **6**, 965–969 (2010)

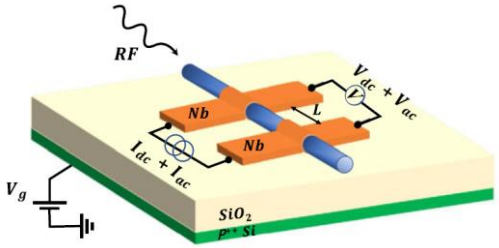

- Inverse a.c. Josephson effect

$$V(t) = V + V_0\cos(\omega' t + \theta)$$

$$I_s = I_c \sum_n (-1)^n J_n \frac{2eV_0}{\hbar\omega'} \sin[(\omega - n\omega') - n\theta + \varphi_0]$$

当$\omega = n\omega'$时： $I_s = (-1)^n I_c J_n \frac{2eV_0}{\hbar\omega'} \sin(\varphi_0 - n\theta)$

DC components: $V_{dc} = n\frac{hf}{2e}$ (Shapiro steps) $(\omega' = 2\pi f)$

- 2π-periodic spectrum

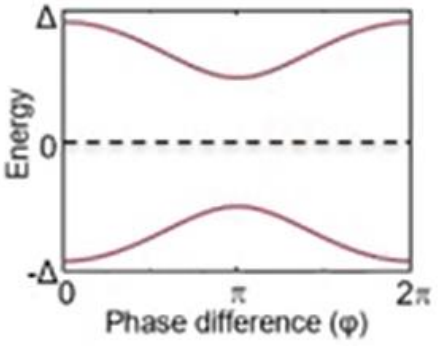

$$I = \frac{2e}{\hbar}\frac{\partial E}{\partial \varphi} = I_0 sin\varphi$$

2π-periodic

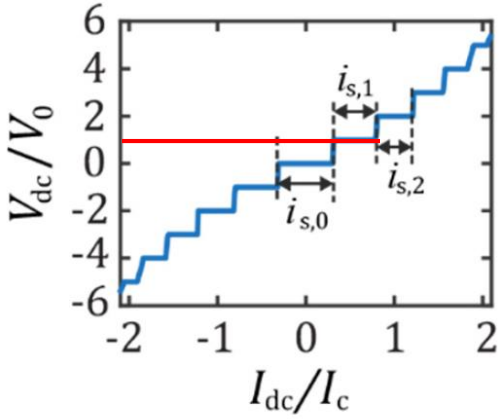

Phys. Rev. B **103**, 235428 (2021)

4π-periodic supercurrent and even-integer Shapiro steps

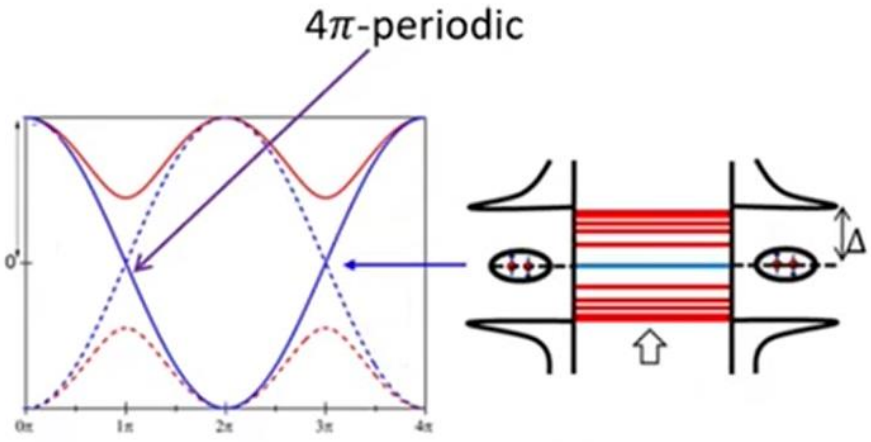

Majorana zero energy mode

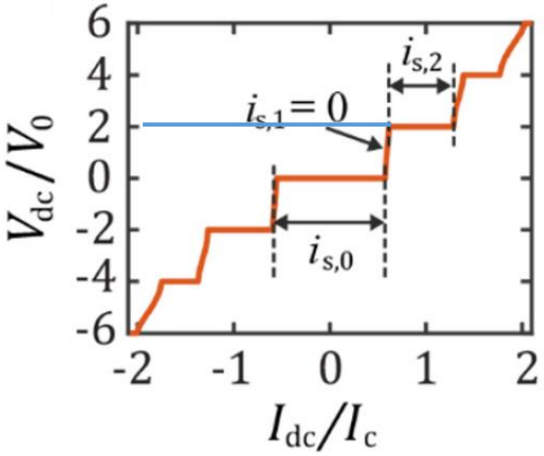

Majorana = “half state”

$$I_{MBS} = \frac{2e}{\hbar}\frac{\partial E}{\partial \varphi} = I_0 sin\frac{\varphi}{2}$$

4π-periodic

$$V_{dc} = \boxed{2n}\frac{hf}{2e}$$

Shapiro step at even-integer

4π-periodic supercurrent from surface states

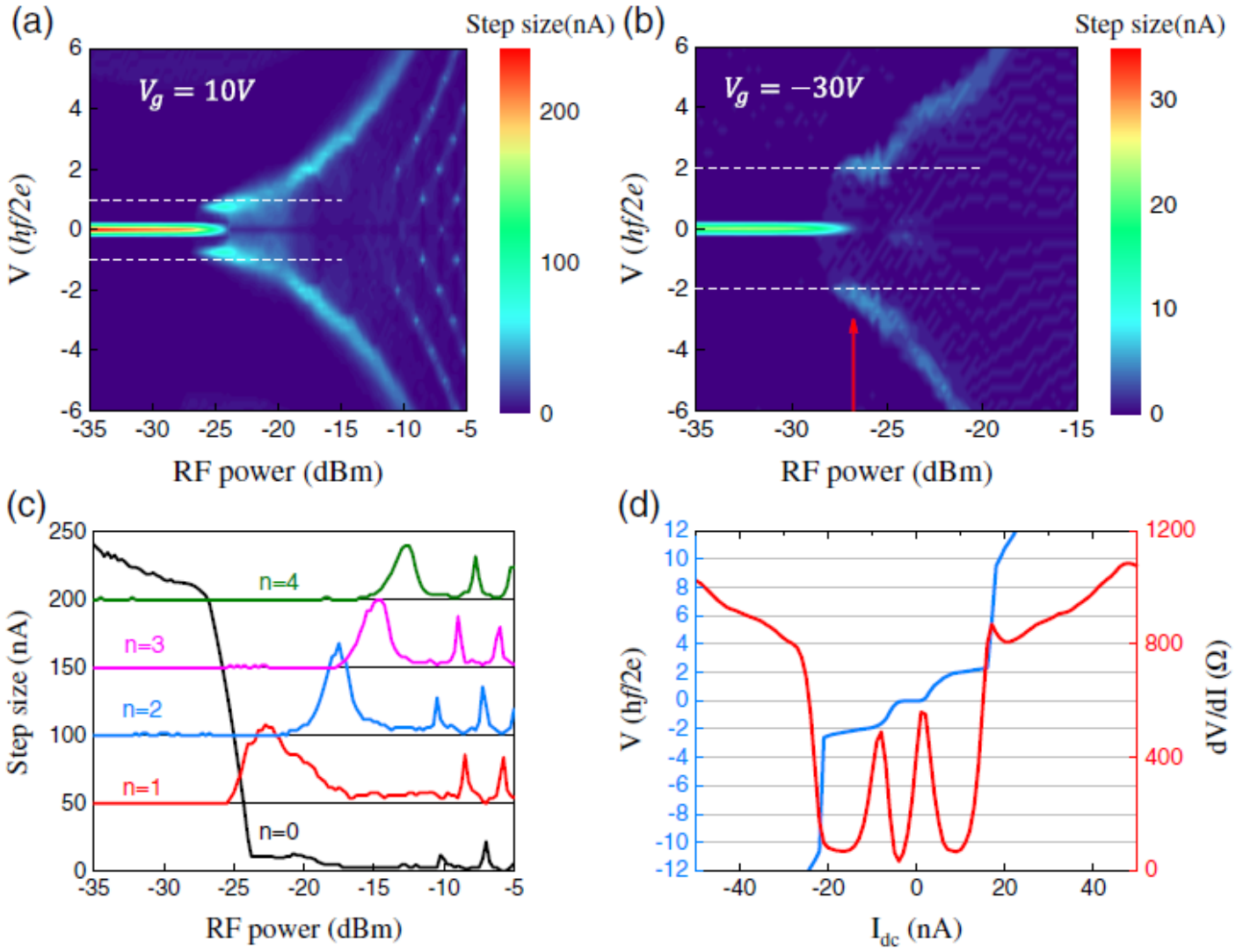

An-Qi Wang[†], **Cai-Zhen Li**[†] *et al.* ***Phys. Rev. Lett.*** 121, 237701 (2018).

3. Transport properties in Cd_3As_2 based Josephson junctions

I. Gate-tunable topological superconductivity and 4π-periodic supercurrent (in Cd_2As_2 nanowires)

II. Fermi-arc supercurrent oscillations (in Cd_3As_2 nanoplates)

III. Higher order topological hinge states (in Cd_3As_2 nanoplates)

Nb-Cd_3As_2-Nb Josephson junctions

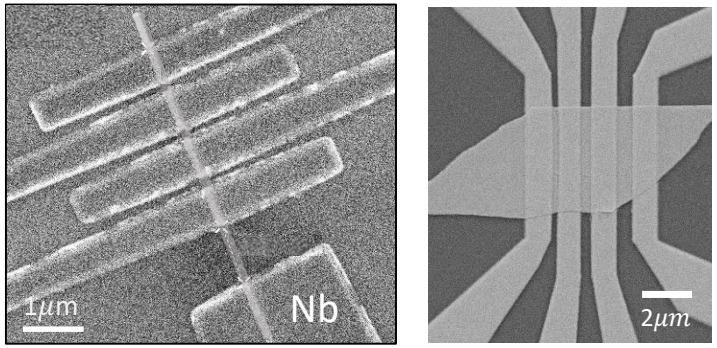

Nb-Cd_3As_2-Nb Josephson junction

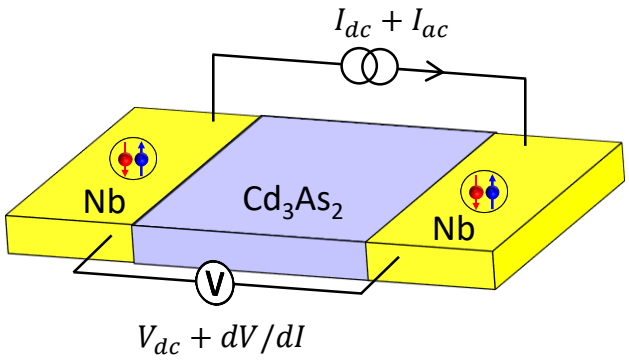

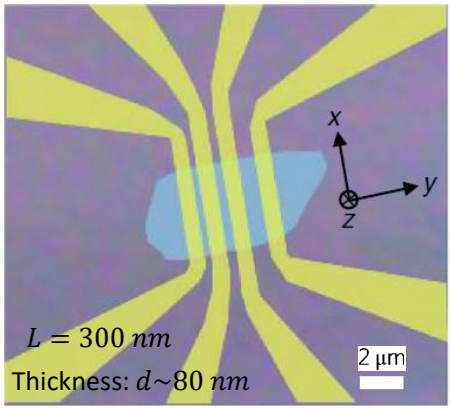

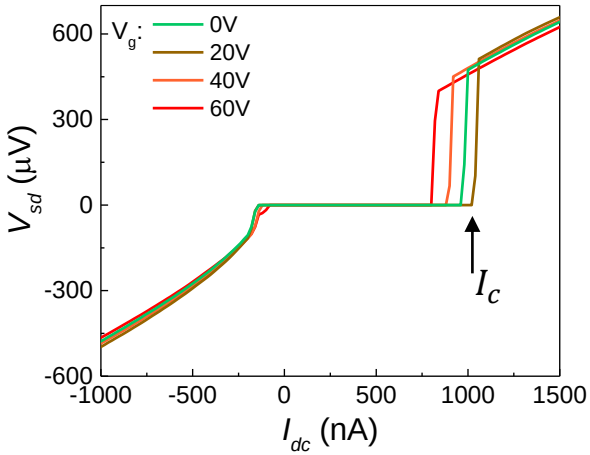

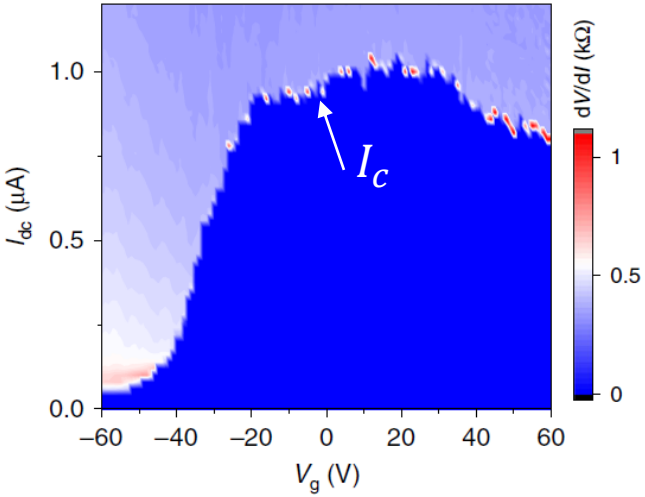

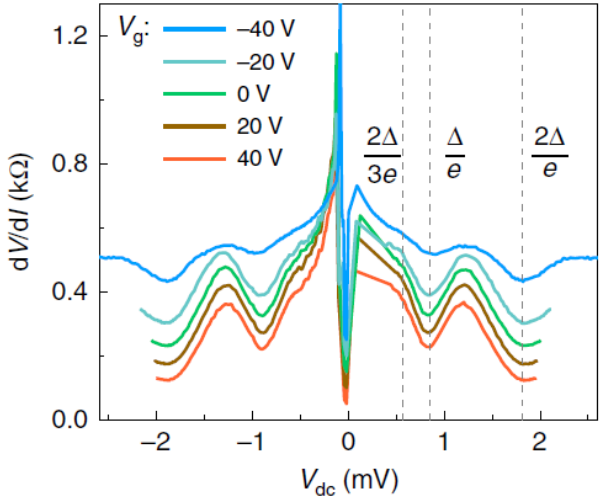

Induced SC gap:

$\Delta = 0.9\ meV$

- Gate-tunable supercurrent
- Multiple Andreev Reflection (MAR)

Cai-Zhen Li †, An-Qi Wang† *et al.* ***Nat. Commun.*** 11, 1150 (2020).

Supercurrent oscillations under parallel B

Two-channel transport

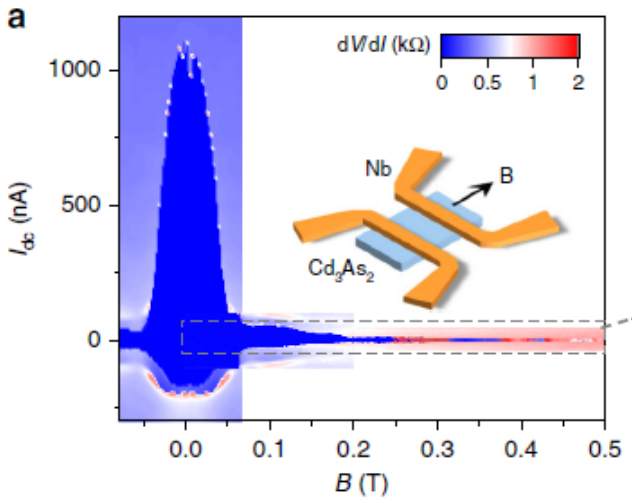

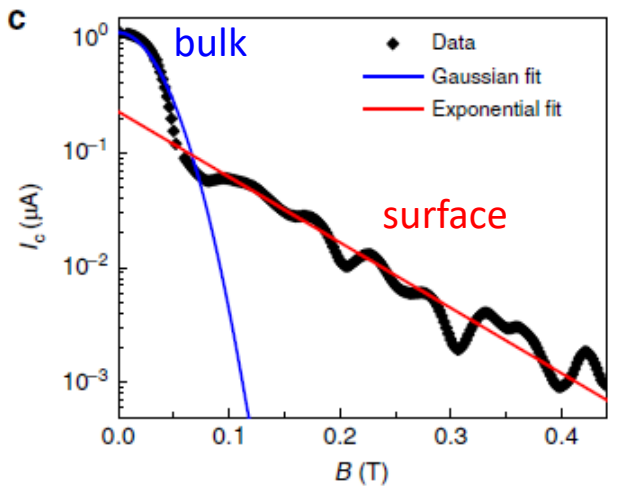

I_c oscillations at higher fields

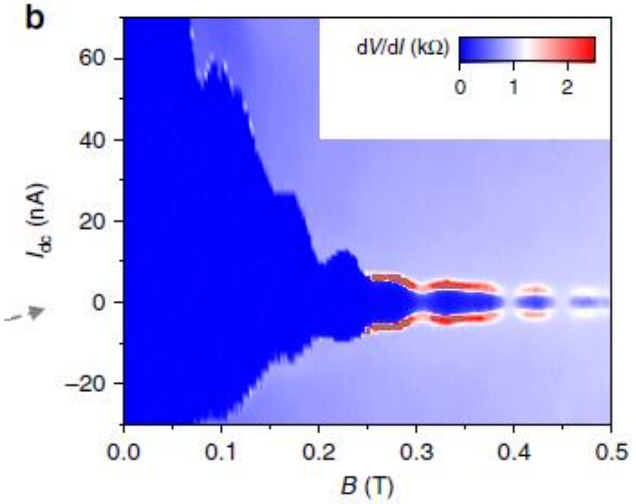

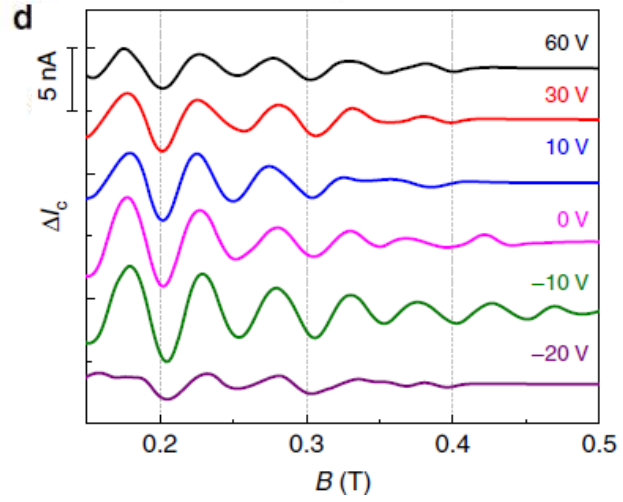

Two-channel transport: bulk and surface

Applying a magnetic field (0.1T) to suppress the bulk-carried supercurrent

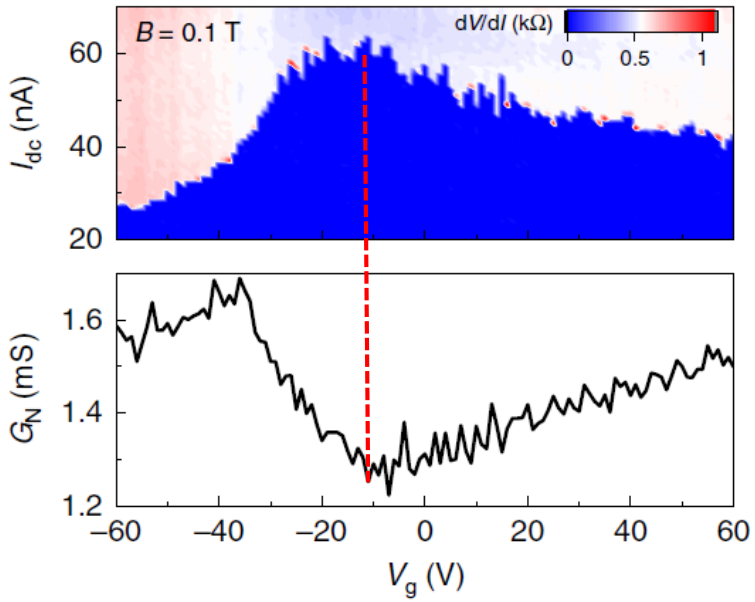

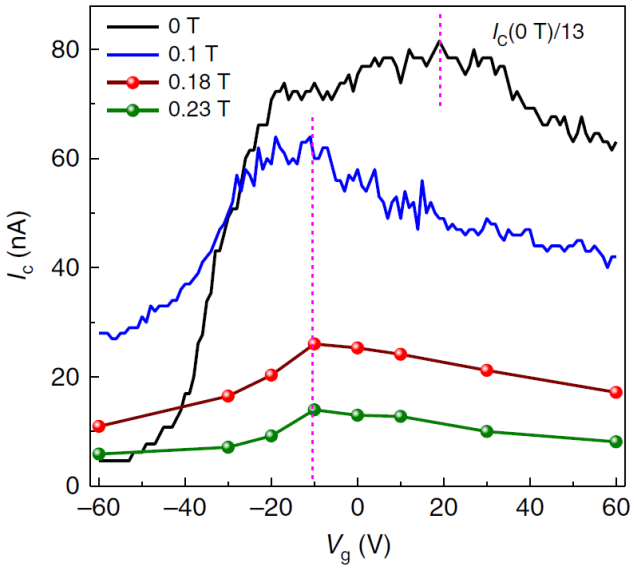

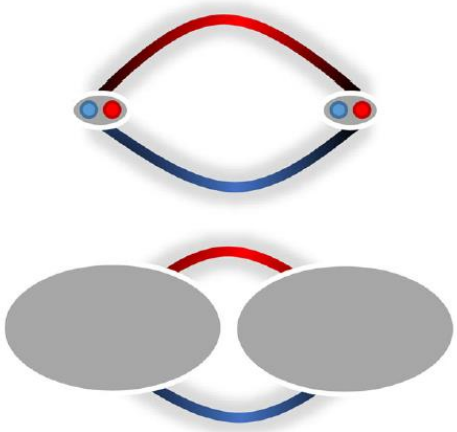

Near Dirac point ⇒ At $V_g = -10V$:

I_c, maximum

G_N, minimum

Far from Dirac point

Supercurrent oscillations: orbital effect

- Zeeman effect: finite momentum pairing (excluded)
- magnetic misalignment (excluded)
- spin-orbital phase shift (excluded)
- **orbital effect**

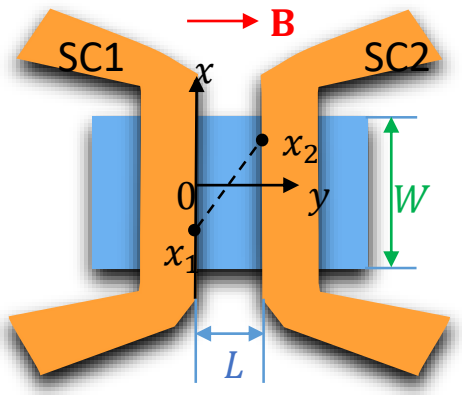

orbital phase: $\frac{2\pi}{\Phi_0}\int_{x_1}^{x_2}\mathbf{A}\cdot dl$

phase difference between x_1 and x_2:

$$\phi_1(x_1)-\phi_2(x_2)=\frac{\pi\mathbf{B}(x_1-x_2)t}{\Phi_0}$$

$$I^{\text{surface}}(\Delta\phi,\mathbf{B})$$

$$=\int_{-\frac{W}{2}}^{\frac{W}{2}}\int_{-\frac{W}{2}}^{\frac{W}{2}}dx_1dx_2\,\frac{1}{\mathbf{r}^{\varepsilon}}\sin\left(\Delta\phi+\phi_1(x_1)-\phi_2(x_2)\right)$$

where $\mathbf{r}=\sqrt{L^2+(x_1-x_2)^2}$

ε denotes the phase coherent strength along the x direction

t: nanoplate thickness

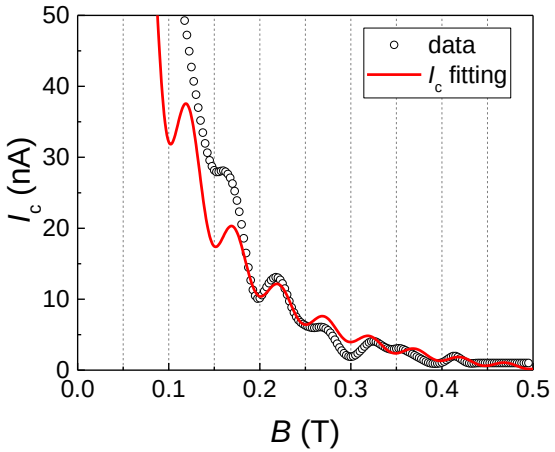

3. Transport properties in Cd_3As_2 based Josephson junctions

I. Gate-tunable topological superconductivity and 4π-periodic supercurrent (in Cd_2As_2 nanowires)

II. Fermi-arc supercurrent oscillations (in Cd_3As_2 nanoplates)

III. Higher order topological hinge states (in Cd_3As_2 nanoplates)

Nb-Cd_3As_2-Nb Josephson junctions

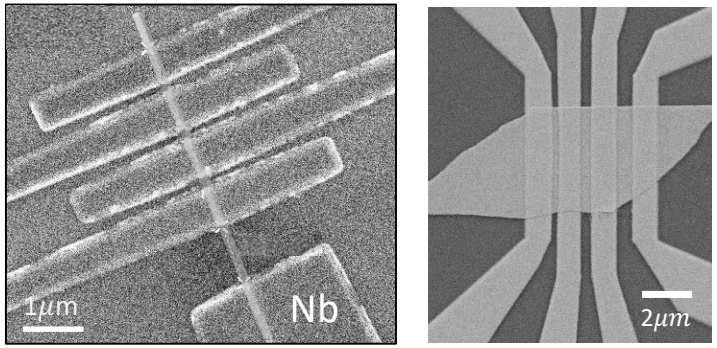

Higher order topological states

A d-dimensional system n-th order topological phase holds gapless states that live on $(d-n)$ dimensional subsystems.

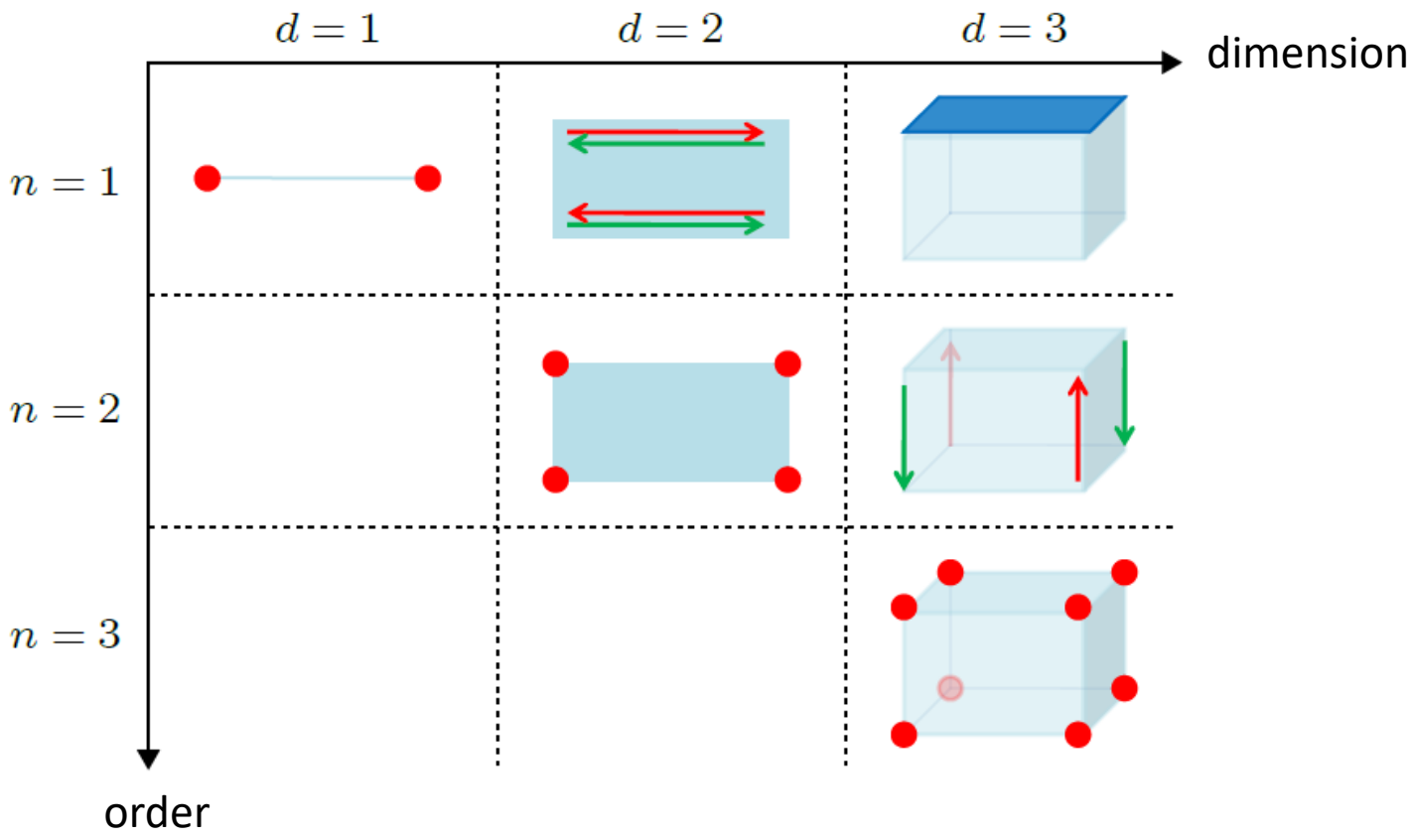

Acta Physica Sinica, 68, 226101 (2019)

Cd_3As_2: a Higher order topological semimetal

- Phys. Rev. B 99, 041301(R) (2019) [Bitan Roy *et al.*]

Higher-order topological phases: A general principle of construction

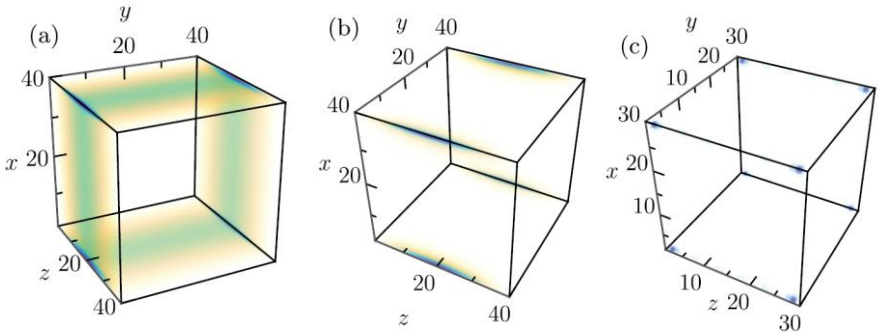

To summarize, we here present a general principle for constructing HOT phases, including gapped [46] and gapless representatives. In particular, we illustrate the higher-order generalization of a topological Kondo insulator (see Fig. 1), TDSMs (see Figs. 2 and 3), which can be realized in Cd_3As_2 [51], Na_3Bi [52], and a NLSM (see Fig. 4), relevant for Ca_3P_2 [53], when subjected to lattice deformations thereby reducing the symmetry. This construction can also be applied to gapless

- Nat. Commun. **11**, 13, 627 (2020). [B. Andrei Bernevig *et al.*]

Strong and fragile topological Dirac semimetals with higher-order Fermi arcs.

- The surface Fermi arcs in Dirac semimetals can be disconnected and removed without breaking a symmetry or closing a gap, therefore are not topological consequences of the bulk Dirac points themselves.
- The surface states appear due to the topology of high symmetry planes, and are not required to connect the surface projections of the bulk Dirac points.

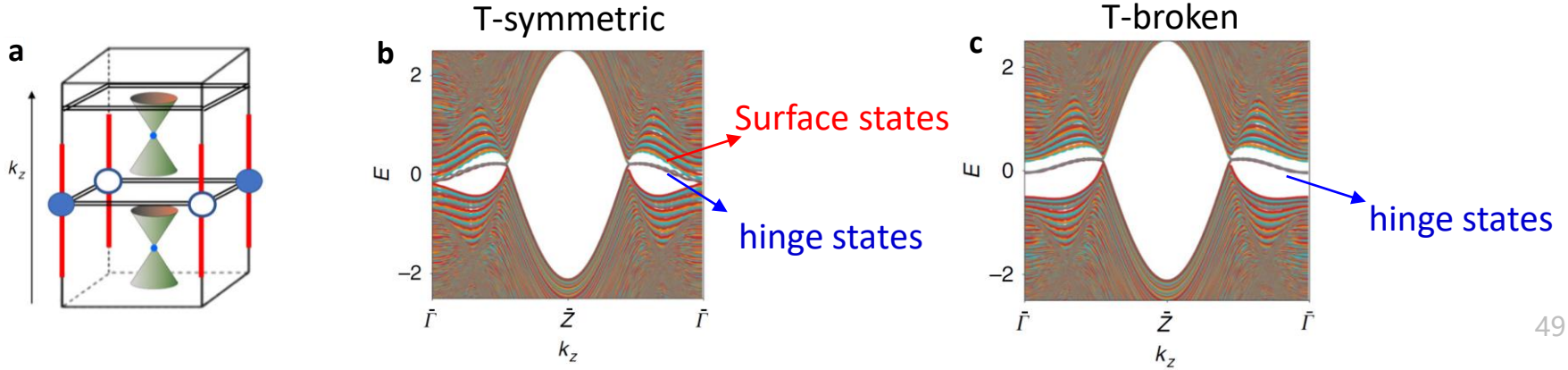

Transport modes filter by supercurrent interference

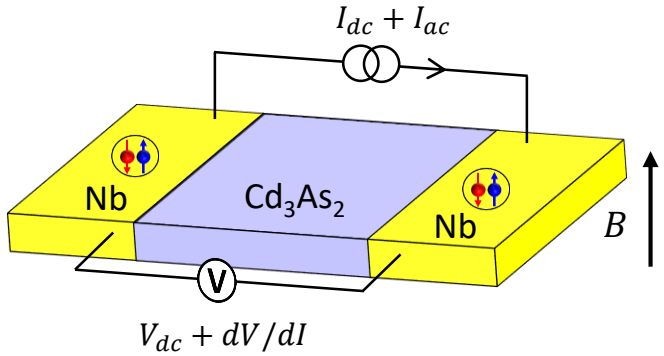

$$I_c(B) = |\mathcal{J}_c(B)|$$

$$= \left| \int_{-\infty}^{\infty} J_c(x) exp(i2\pi L_{eff} B\, x/\Phi_0) dx \right|$$

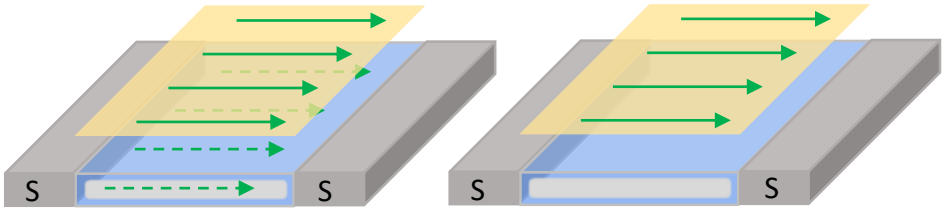

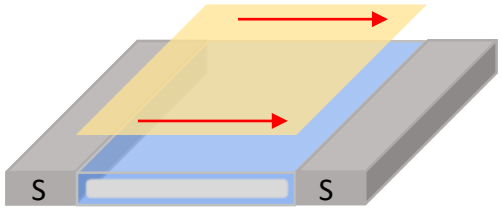

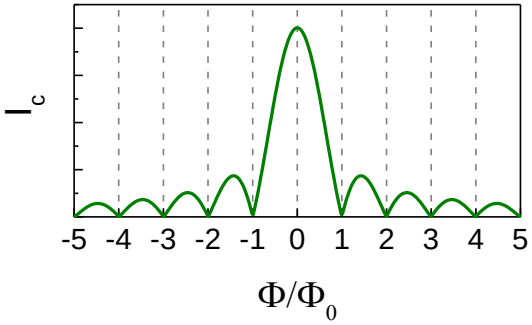

Fraunhofer pattern

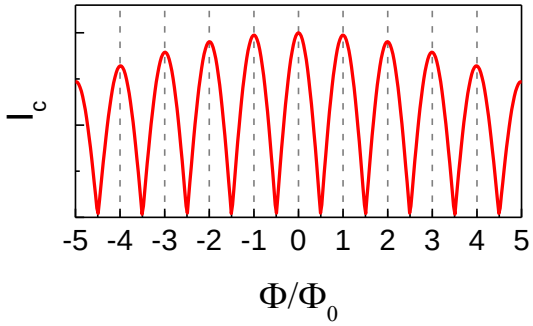

SQUID pattern

(superconducting quantum interference device)

Fraunhofer pattern under perpendicular B

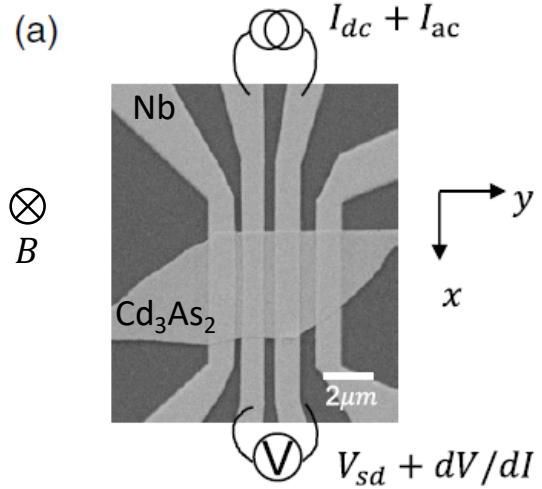

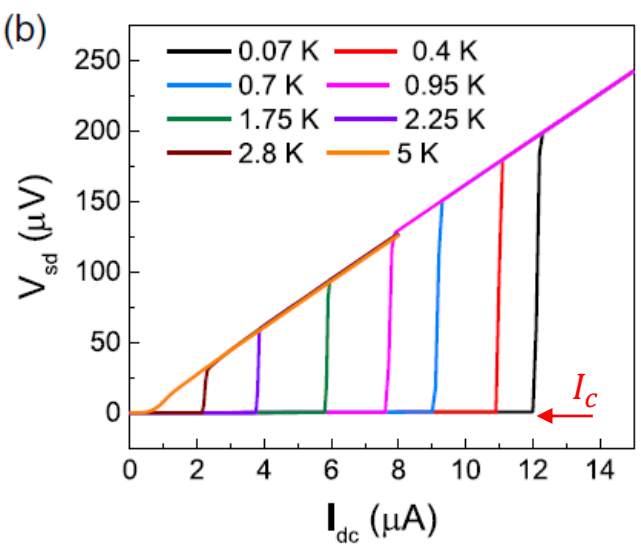

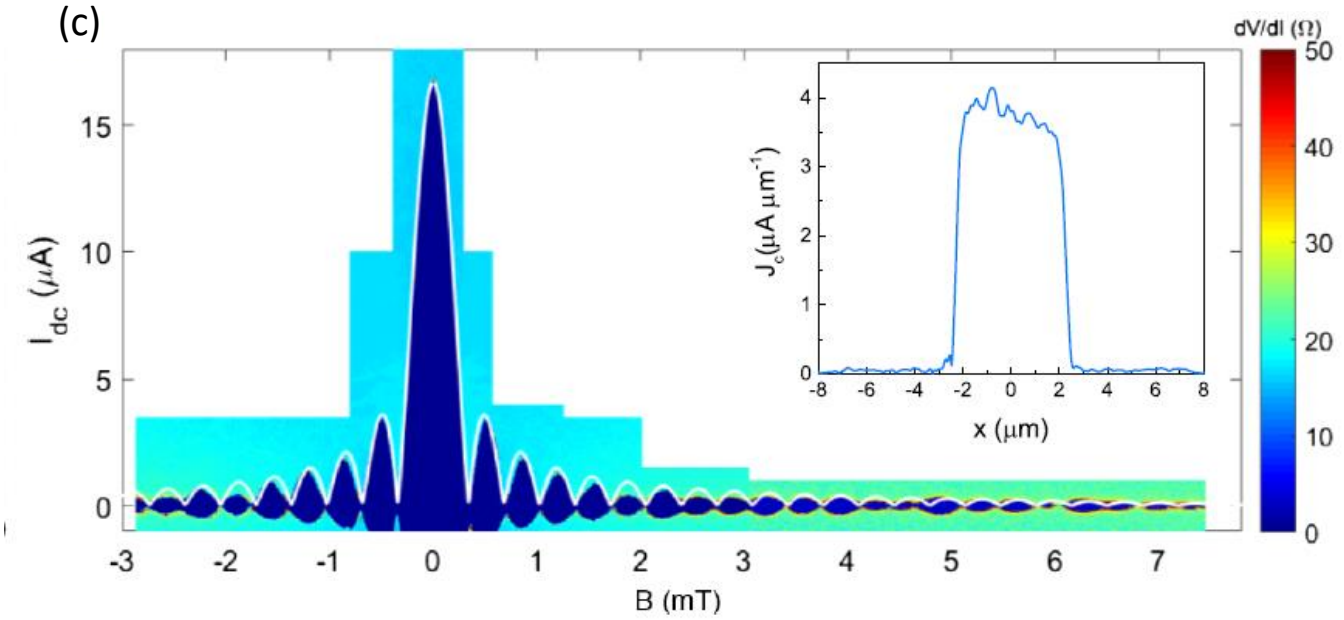

$$L = 500\ nm$$

$$I_c(B) = I_{c0}\left|\frac{\sin(\frac{\pi BS}{\Phi_0})}{\frac{\pi BS}{\Phi_0}}\right|$$

SQUID pattern in a long junction

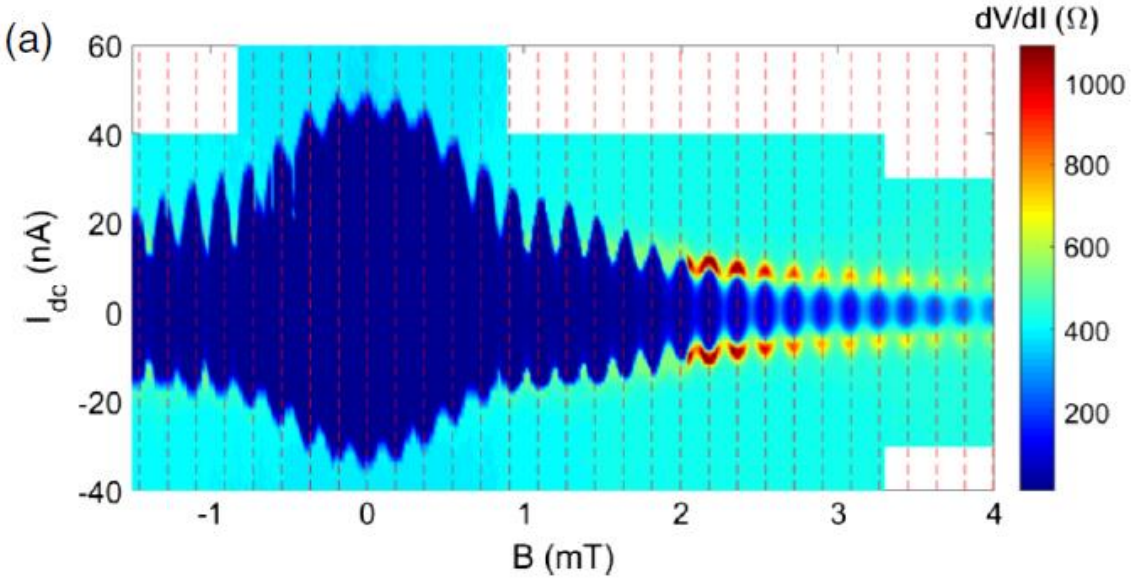

$L = 1\ \mu m$

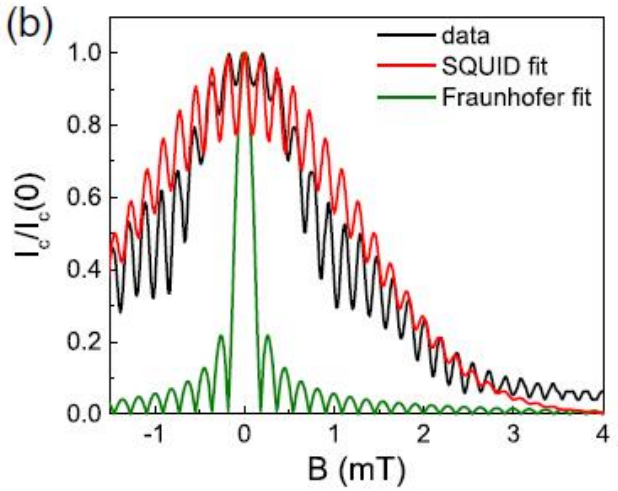

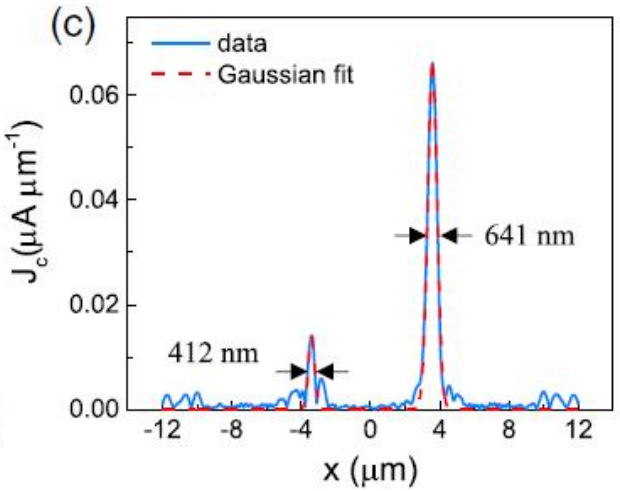

Reducing electronic transport dimension to topological hinge states by increasing device size

Increasing junction length

$L = 500\ nm$, 3D

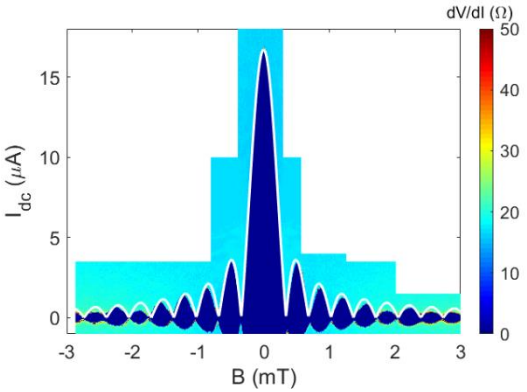

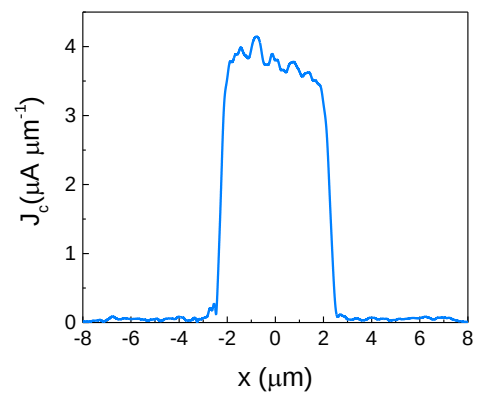

$L = 800\ nm$, 2D

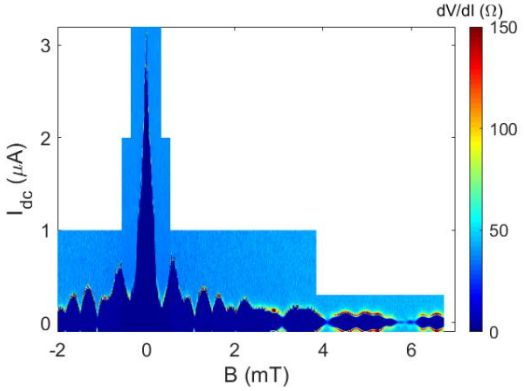

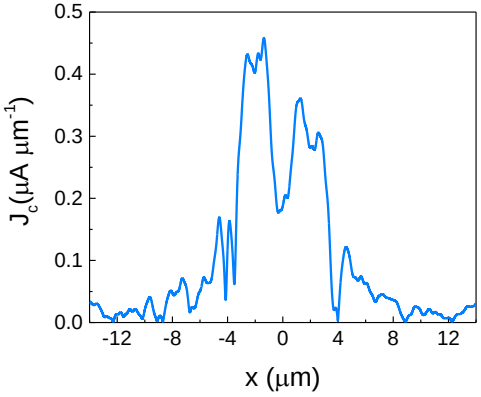

$L = 1\ \mu m$, 1D

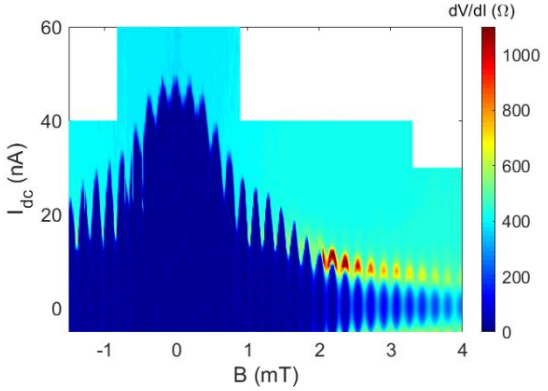

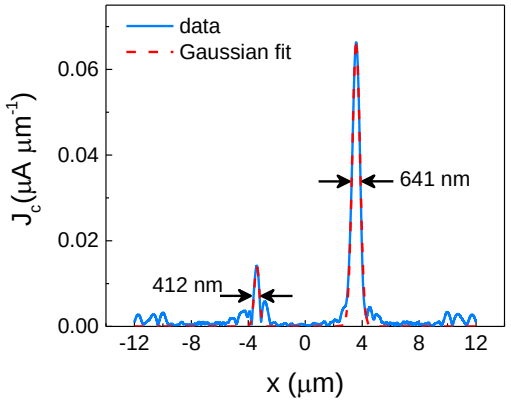

Superconducting coherence length: $l_{\varphi}^{3D\ bulk} < l_{\varphi}^{2D\ surface} < l_{\varphi}^{1D\ hinge}$

Summary

Transport properties of Cd_3As_2 nanostructures

I. Chiral anomaly effect in Cd_3As_2 nanowires and nanoplates

II. Aharonov-Bohm oscillations in Cd_3As_2 nanowires

III. Two carrier transport in Cd_3As_2 nanoplates

Transport properties of Nb-Cd_3As_2-Nb Josephson junctions

I. Gate-tunable topological superconductivity and 4π-periodic supercurrent (in Cd_2As_2 nanowires)

II. Fermi-arc supercurrent oscillations (in Cd_3As_2 nanoplates)

III. Higher order topological hinge states (in Cd_3As_2 nanoplates)

Thank you for your attention!